AD-A096 283 MAX-PLANCK-INST FUER CHEMIE MAINZ (GERMANY F R) F/G 7/5
LABORATORY MEASUREMENTS OF PHOTOLYTIC PARAMETERS FOR FORMALDEHY--ETC(U)
NOV 80 G K MOORTGAT, W KLIPPEL, K H MOEBUS DOT-FA78WA-4264
UNCLASSIFIED FAA/EE-80-47 NL

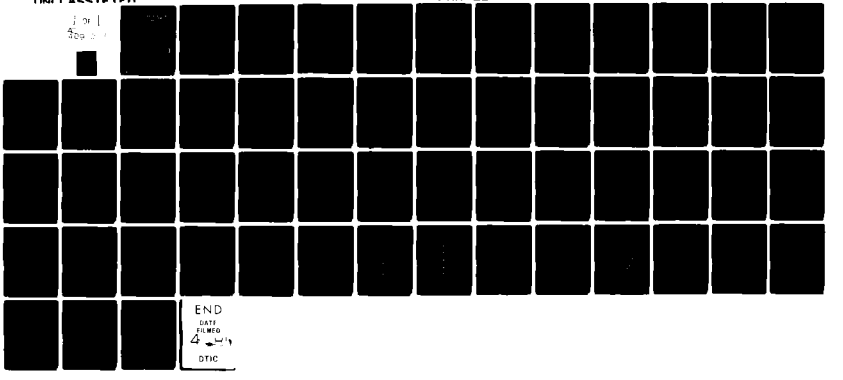

END
DATE FILMED
4-81
DTIC

FAA-EE-80-47

U.S. Department of Transportation
Federal Aviation Administration

LABORATORY MEASUREMENTS OF PHOTOLYTIC PARAMETERS FOR FORMALDEHYDE

Office of Environment and Energy
Washington D.C. 20591

November 1980

G.K.Moortgat
W.Klippel
K.H.Möbus
W. Seiler
P. Warneck

Technical Report Documentation Page

1. Report No.	2. Government Accession No.	3. Recipient's Catalog No.
(19) (18) FAA-EE-80-47	AD-A096 283	

4. Title and Subtitle (6)
LABORATORY MEASUREMENTS OF PHOTOLYTIC PARAMETERS FOR FORMALDEHYDE.

5. Report Date
November 1980

6. Performing Organization Code
12157

7. Author(s) (10)
G.K. Moortgat, W. Klippel, K.H. Moebus, W. Seiler, P. Warneck

8. Performing Organization Report No.

9. Performing Organization Name and Address
Max-Planck-Institut für Chemie (Otto-Hahn-Institut)
Abteilung Chemie der Atmosphäre
D-6500 Mainz, Federal Republic of Germany

10. Work Unit No. (TRAIS)

11. Contract or Grant No. (15)
DOT-FA78WA-4264 new

12. Sponsoring Agency Name and Address
U.S. Department of Transportation, Federal Aviation Administration
Washington, D.C. 20591

13. Type of Report and Period Covered (9)
Final Report.

14. Sponsoring Agency Code

15. Supplementary Notes

16. Abstract

The photodecomposition of formaldehyde has been studied experimentally under simulated atmospheric conditions at temperatures 220 and 300 K. Quantum yields for H_2 and CO formation are reported for the spectral region 270 - 355 nm and are used to derive quantum yields for the two primary photolytic pathways. Absorption cross sections are also reported for a number of different temperatures. The data have been used to calculate CH_2O photodissociation coefficients in the atmosphere as a function of altitude.

17. Key Words	18. Distribution Statement
Formaldehyde Quantum Yields Photodissociation Coefficients	

19. Security Classif. (of this report)	20. Security Classif. (of this page)	21. No. of Pages	22. Price
Unclassified	Unclassified		

Form DOT F 1700.7 (8-72) Reproduction of completed page authorized

Laboratory Measurements of Photolytic Parameters for Formaldehyde

G.K. Moortgart, W. Klippel, K.H. Möbus, W.Seiler
and
P. Warneck

Max-Planck-Institut fuer Chemie (Otto-Hahn-Institut)

Mainz, Federal Republic of Germany

Table of Contents

Summary

The photodecomposition of formaldehyde in air has been investigated in the laboratory at two temperatures: 300 and 220 K. Quantum yields for the formation of CO and H_2 were determined at nine wavelengths in the spectral region 270-355 nm, each wavelength being isolated by a monochromator with 5 nm spectral resolution. From the experimental data, the quantum yield curves for the two photolytic pathways

$$CH_2O + h\nu \longrightarrow H + HCO \qquad \phi_1$$
$$\longrightarrow H_2 + CO \qquad \phi_2$$

were obtained as a function of wavelength. The total quantum yield $\phi_1 + \phi_2$ is identical with the CO quantum yield. It is unity and essentially independent of temperature and pressure at wavelengths less than 330 nm. At longer wavelengths the CO quantum yield decreases due to quenching. At 353 nm and one atmosphere pressure the CO quantum yields are 0.26 for a temperature of 300 K, and 0.11 for 220 K. The corresponding quenching constants in terms of number density are $\alpha^n = 1.09 \cdot 10^{-19}$ cm^3/molecule and $2.47 \cdot 10^{-19}$ cm^3/molecule at 300 K and 220 K, respectively.

Absorption cross sections for formaldehyde were measured: (a) with 0.5 nm spectral resolution to derive data for the calculation of photodissociation coefficients, and (b) with 5 nm spectral resolution to obtain cross sections needed for the evaluation of quantum yields.

Based on the experimental data, but neglecting the temperature effect of quenching in the 330-360 nm wavelength region, CH_2O photodissociation coefficients were calculated as a function of altitude for three solar zenith angles (30, 50, 70 degrees). Raleigh scattering and an assumed ground albedo of 0.3 were included in the computational routine. Photodissociation coefficients J_1, J_2 and $J_1 + J_2$ are tabulated in intervals of 1 km for the 0-50 km altitude range.

Introduction

This Final Report under Contract No. DOT-FA78-WA-4264 describes experimental data on absorption cross sections and quantum yields for the two pathways of formaldehyde photodecomposition in the spectral region pertinent to the atmosphere in accordance with the work statement of the contract. In particular, quantum yield data for room temperature and stratospheric temperature are reported. A later amendment of the original work statement calls for the computation of photodissociation coefficients (J values) based upon the results of the measurements, and these data will also be provided here. The following text is subdivided into three sections which describe, in turn, the experimental arrangements used, the results obtained for absorption cross sections and quantum yields together with a short critique, and the results of the computations. The application of these data to problems of atmospheric chemistry will not be discussed.

Experimental Techniques

(a) Absorption Cross Sections.

A commercial double beam spectrophotometer was used. The instrument develops a single light beam from a deuterium lamp (for the wavelength region below 400 nm) in conjunction with a Czerny-Turnertype scanning monochromator of moderate resolution. The light beam is then passed alternately through a sample cell and a reference cell and directed onto one and the same photomultiplier by means of two sychronized rotating mirrors. The photomultiplier signal is amplified, and electronically processed to retrieve sample and reference signals. The logarithm of their ratio, appropriately factored, is derived electronically to yield directly the absorption coefficient as the final electric output signal. Calibration of wavelength scale was performed by using the two sharp emission lines of the deuterium lamp spectrum at 486.0 and 656.1 nm as standards. Calibration of the absorption cross section scale was checked using filters with known transission.

A set of optically matched sample cells made of fused quartz were used. Their optical length was 80 mm. These cells were provided with

jackets for a heating or cooling fluid, as well as with evacuated and sealed double windows on each end to eliminate frosting. The moisture content of the cell compartment was in addition reduced by flushing with dry nitrogen. One cell was evacuated and sealed off and served as a reference cell, the other one was connected to a gas handling system. Each cell was held in position by four prongs so that thermal heat losses were minimized. Ethylalcohol served as a cooling fluid. It was circulated through a conventional thermostat connected to a dry ice supply. Temperatures down to 200 K could be maintained in this way. A second thermostat equipped with a heater was used to reach temperatures of about 370 K. The cell temperature was measured by a set of platinum resistance thermometers located at the inflow and outflow junctions of the cell's jacket.

Formaldehyde was prepared from paraformaldehyde by heating it to 150^{o} C in an evacuated system keeping the pressure at 15 torr. The vapor was collected in a trap cooled by dry ice. It was subsequently purified by trap to trap destillation and finally stored in a cylindrical trap kept at the temperature of liquid nitrogen. The storage trap was kept in the dark and was connected to a handling manifold of the type shown in Figure 1. Only teflon stoppered cocks or stainless steel bellows valves were used in constructing the manifold. From the storage trap, formaldehyde was admitted either directly into the absorption cell or was brought into an evacuated mixing vessel where nitrogen was added to produce CH_2O - N_2 mixtures of known mixing ratios. In either case, the number density of formaldehyde in the cell was calculated from the measured pressures and temperature.

With pure formaldehyde in the absorption cell, a decrease of the working pressure with time was initially noted, but as the number of experiments in sequence rose, the cell became conditioned. Then, the data obtained were quite reproducible, indicating that the adsorption-desorption processes occuring at the walls had become stationary. With pure formaldehyde in the cell, the zero line was checked after each run by freezing the formaldehyde into a freeze trap. The background was noted to build up after a series of runs. This effect is assumed

to result from the polymerization of formaldehyde on the windows of the cell. The background could be removed again by pumping on the cell for a prolonged period of time. The change in zero line with time was taken into account in two ways: (a) by taking data only over short time intervals, as with formaldehyde; and (b) by appropriate corrections for the increasing background when slowly scanning the spectrum over the entire spectral range 240-370 nm. One scan required about 20 minutes. The latter procedure was used both with pure formaldehyde and with CH_2O-N_2 mixtures. A comparison of data obtained by both procedures in the case of pure formaldehyde gave consistent results.

(b) Quantum Yields

Mixtures of formaldehyde in air were photolyzed in a conventional manner in cylindrical quartz cells. Ultraviolet light, generated by a 150W-Xenon arc lamp, passed first through a distilled water i.r. filter, and was then focussed onto the entrance slit of an f/2 Jobin-Yvon monochromator. This instrument uses a holographic grating eliminating image errors whereby the useful light intensity is increased over that of conventional Czerny-Turner type monochromators. The widths of the entrance and exit slits were set to 2 mm each, so that a spectral resolution of 5 nm halfwidth was obtained. The light emerging from the monochromator was collimated by means of a quartz lens to a parallel beam width coinciding with the internal diameter of the photolysis cell. After having passed the cell, the light beam fell onto a calibrated thermopile which served to monitor the radiation and to measure its absolute flux. A small fraction of the radiation emitted from the light source was deflected upon a photodiode whose signal was used to regulate the lamp power supply keeping its photon flux constant to within 0.2% during the duration of the photolysis.

Formaldehyde was prepared as described in the previous section. Mixtures of formaldehyde and air were prepared in the gas handling system shown in Figure 2. Synthetic air was freed from hydrocarbons, CO and H_2 by a combination of traps containing molecular sieve and hopcalite. A known amount of formaldehyde was first isolated in a calibrated volume and then expanded into an evacuated 16.3 liter storage vessel. Air was added subsequently until a pressure of about 800 torr

was reached. The gas mixture was kept in the dark and heated to 100°C to prevent losses of formaldehyde by polymerisation. The formaldehyde content of the mixture was checked at the beginning of each photolysis experiment by withdrawing a sample with a syringe through a gas-tight silicone septum and injecting it into the port of a gas chromatograph equipped with a flame ionisation detector (lower detection limit 0.5 ppmv of CH_2O). The amount of formaldehyde present was always found to be in agreement with that calculated from the mixing procedure.

The photolysis cells were made of quartz. The internal photolysis space was cylindrical, 10 cm in length, 1.0 cm in diameter. The cells were provided with a jacket for a cooling fluid and dual windows with evacuated intermediate space on each end to reduce frosting. A slight amount of heating of the outer windows was found necessary to achieve a complete frostfree operation. Cooling fluids and thermostatting was similar to that described in the previous section. Two cells were used in parallel. One served as the photolysis cell proper, the other as a blanc cell. At the beginning of a run, both cells were filled with formaldehyde-air mixture via a set of solenoid switching valves in the arrangement shown in Fig.3. The set-up allowed the direct transfer of gases from the sample cells to a gas chromatograph equipped with a nickel catalyst which converts carbon monoxide to methane for the subsequent detection by flame ionization. Only a few runs were made using this procedure, mainly because it did not allow the measurement of the photolysis product hydrogen. In the majority of experiments samples were withdrawn from the photolysis cell by means of a gas-tight syringe whose needle was inserted into the photolysis cell via a silicone septum. The gas sample was then injected into the entrance port of the H_2 and CO analyzer to be described below. Transfer of sample to the gas chromatograph was used also to check on the formation of products other than CO and H_2, such as formic acid, but none were found.

The schematics of the CO/H_2-analyzer is shown in Figure 4. For the present purpose a discontinuous operation is appropriate. A stream of CO/H_2 free air is flowed via an injection port into a molecular sieve column where hydrogen and carbon monoxide are

separated, then into a mercury oxide converter heated to 250°C. Here CO and H_2 undergo reaction liberating elementary mercury which is then detected by 253.7 nm resonance absorption in an optical cuvette. The signal derived from a photo-cell is compared to a reference signal, amplified, and recorded. A typical recorder output is shown in Figure 5. The instrument is calibrated with mixtures of CO or H_2 in air, prepared by dynamic dilution methods. Compressed air stored in steel cylinders, carefully selected to contain carbon monoxide and hydrogen at mixing ratios of about 200 and 500 ppbv, respectively, were used as secondary standards. These mixtures were found to be stable over extended periods of time. They were used to check upon instrument calibration each time a photolyzed mixture was analysed.

Experimental Results

(a) Absorption cross sections

Spectra were measured for two slit settings providing wavelengths resolutions of 0.5 nm and 5 nm. Absorption cross sections for the former setting were used in the calculation of photodissociation coefficients. Cross sections for the latter resolution were required in conjunction with the photolysis experiments for the calculation of quantum yields.

Figure 6 shows the absorption spectrum of formaldehyde obtained at 0.5 nm resolution for two temperatures, room temperature and 210 K. There are no noticable differences in the two spectra, so that from visual inspection the effect of temperature must be small. It is clear that the (high resolution) rotational intensity distribution must change with temperature, but the change does not seem to be great enough to affect significantly the shape of the bands observed here with rather modest resolution. Absorption cross sections were derived from the maxima of the bands of spectra obtained at four different temperatures, using the relation $\sigma = D\ (\log 10)/nL$ where $D = \log^{10} I_0/I$ is the decadic extinction recorded, L is the cell length, and $n = 2.69 \cdot 10^{19} \cdot 273.2\ p/760\ T$ with the pressure p given in torr and the temperature T in Kelvin. The linearity of extinction with pressure was checked for a few bands and was found satisfactory. A working pressure of

about 10 torr was then chosen in the determination of absorption cross sections. Four sets of cross section data obtained at 214.6 K are given in Table 1 to indicate the reproducibility of the data. The standard deviation indicates a precision of about two percent. Data obtained at various temperatures in the range 211 - 362 K are compiled in Table 2. The results are also plotted in Figures 7 and 8 for the 4^1 and 4^3 band progressions. Inspection of the data shows that for most bands the absorption cross sections are not affected much by temperature, while for some bands the cross sections increase by a few percent when the temperature is decreased from 362 to 211 K. The percentage is indicated on the right hand side of Figures 7 and 8. Even for these data the change is sufficiently small in most cases to be negligible to a first approximation. Exceptions occur with the bands 4^1, 2^74^1, 4^3 and particularly with the unresolved combination of $2^44^3 + 2^54^1$ bands. It appears that an appreciable trend with temperature is established only for about 7 bands out of 31. Since even for these bands the percentage change for temperatures between 300 and 310 K is less than 20%, we consider it justifyable to neglect it for the purpose of calculating photodissociation coefficients.

Data at temperatures above room temperature, although not required by contract, were taken mainly because our previous photolysis data relied on cross section measurements at 70°C. This temperature was chosen to eliminate a conceivable polymerisation of formaldehyde on the walls of the absorption cell and to permit high vapor pressures of H_2CO. The 70°C results were then applied in the derivation of quantum yields at room temperature. This procedure becomes questionable, if the effective cross sections were strongly temperature-dependent. The present results allay such fears and show that the previous procedure was entirely justified.

We must stress that the absorption cross sections given here are effective absorption cross sections. A resolution of 0.5 nm is too coarse to reveal the distribution of rotational lines contained within an absorption band. The calculated absorption strength thus averages over many rotational lines and the regions of minimal absorption in-between. For the evaluation of photodissociation coefficients one would have to take, in principle, the absorption cross sections and

quantum yields for each rotational line and then sum over all lines. Such a detailed knowledge is beyond present experimental capabilities, and if it were available from laboratory measurement it could not be applied because the intensity distribution of the solar spectrum is not sufficiently resolved. The techniques applied here provide integral values for a number of coarse wavelength intervals emphasizing the principal bands of formaldehyde.

For reasons of providing sufficient intensity, the photolysis experiments were done with a coarse spectral resolution of 5 nm. At this resolution the spectrum, shown in Figure 9, consists of nine broad bands. Absorption cross sections effective for these conditions are required in the calculation of quantum yields. In contrast to the data described above, the results obtained at 5 nm resolution indicated a pressure effect for some of the bands - both at room temperature and at low temperatures - in that the absorption cross sections decreased with increasing pressure of formaldehyde. The magnitude of the effect is shown in Figures 10 and 11 for data obtained at 298 K, and in Figures 12 and 13 for data obtained at 220 K. Experiments were performed both for pure formaldehyde and for formaldehyde with about 500 torr of nitrogen added.

The variation of absorption cross sections with pressure for spectra characterized by band structure is a well known instrumental effect resulting from inadequate spectral resolution. At low pressures, only the centers of the rotational lines are attenuated, while with increasing pressure also the wings contribute with lower cross sections so that the spectral average cross section decreases as the pressure is raised. What seems to be surprising is the smoothing effect of nitrogen when added as a buffer gas. In the presence of 400-600 torr of nitrogen, the cross sections vary much less with the partial pressure of formaldehyde. The cause of this effect is probably a pressure broadening of the rotational lines, whereby the sharpness of the lines is diminished, so that the magnitude of the pressure effect is reduced.

Formaldehyde partial pressures used in the photolysis experiments are much lower than those employed in measuring absorption cross sections (<0.076 torr compared to 5-20 torr). Hence, it is necessary

to extrapolate the measured cross sections toward zero pressures. It can be seen from Figures 10-13 that the data obtained with and without nitrogen addition extrapolate to the same zero pressure cross sections. The cross sections thus obtained are listed in Table 3. It can be seen that the difference for the two temperatures is small. Hence, averaged values were employed in the determination of quantum yields.

(b) Quantum yields

The mixing ratios of carbon monoxide and hydrogen which are observed in the sample taken from the photolysis cell at the end of a photolysis run are given by

$$m\ (CO) = \phi\ (CO) I_{abs}/n(M)V$$

$$m\ (H_2) = \phi\ (H_2) I_{abs}/n(M)V$$

where ϕ (CO) and ϕ (H_2) are the quantum yields of CO and H_2 production, respectively, I_{abs} is the total number of photons absorbed by formaldehyde during the photolysis run, n(M) is the total number density of all molecules present in the cell which, due to the small contributions of CH_2O, CO and H_2 is essentially that of air, and V is the total volume of the cell. The number of absorbed photons is given by

$$I_{abs} = I_o \sigma_{eff} n(CH_2O) A\ L\ \Delta t$$

where I_o is the photon flux inside the photolysis cell, A is the area of the light beam illuminating the cell, L is the length of the cell and Δt is the time period of photolysis. The number density of air molecules can be approximated by

$$n(M) = 2.68 \cdot 10^{19} (p/760)(273.16/T)$$

where the pressure p is given in torr as measured, and the temperature T is taken in degree Kelvin. The determination of quantum yields thus requires the measurements of the CO and H_2 mixing ratios, the pressure and temperature in the cell, the light flux and the duration of a photolysis run. The mixing ratio of formaldehyde, the quantities A, L, V and σ_{eff} are auxiliary parameters which were determined independently. The light flux was measured with the thermopile detector

in the rear of the photolysis cell and corrected for attenuation by the quartz windows which was 10% total so that a 5% higher photon flux existed inside the cell compared with that measured behind it.

The complete results obtained from the photon decomposition experiments and the quantum yields deduced from each run are listed in Table 4. We consider first the ratios of hydrogen versus carbon monoxide produced. Averaged values obtained for the two temperatures employed are shown in Figure 14 as a function of wavelength. Our previously published data (Moortgat and Warneck, 1979) are also shown for comparison. Comparison of the data indicates that the influence of temperature on the $\phi(H_2)/\phi(CO)$ ratio is essentially negligible. The present values for both temperatures are somewhat higher, however, than the previous data. At wavelengths greater than 340 nm, a ratio of unity is expected because the decomposition of CH_2O into H_2 and CO is the only energetically allowed process. The present data approach the expected ratio of unity whereas the previous data do not. This problem had been discussed and calibration errors were considered the most likely cause for it. It appears that the calibration error has now been removed, although the procedures applied were the same as previously.

Figures 15 and 16 show the absolute quantum yields obtained for CO and H_2 versus wavelengths. Below 330 nm essentially no pressure effect was observed and data from all runs were taken to compute the averages shown. Above 330 nm where quenching is known to occur, only the data points obtained with pressures near one atmosphere were averaged and entered in the figures. The CO quantum yield in the spectral region 280-330 nm is unity, on average, regardless of temperature. The decrease of quantum yields to values below unity observed previously in the region 280-290 nm has not been substantiated. The previous data points were few, however, and in addition the available light intensities are now much higher whereby errors are decreased. Below 280 nm, also the present experiments indicate a decline of the CO quantum yield. The scatter in the data points is much greater here than at other wavelengths, increasing the uncertainty of the results. Both the decline of intensity and H_2CO cross sections contribute to greater errors.

The somewhat lower results obtained at 220 K are also attributed to measurement uncertainties. The H_2 quantum yields are in very good ageement with the results of Horowitz and Calvert (1978), but slightly higher than our own data particularly at wavelengths below 290 nm for the reasons discussed above.

The CO (and H_2) quantum yields at wavelengths greater than 330 nm obtained at 300 K and atmospheric pressure are in good agreement with the data of Moortgat and Warneck (1979). The pressure dependence was investigated and found to agree with the previous measurements. Figure 17a shows a Stern-Volume plot of $^1/\phi$ (CO) versus p to demonstrate this point for the data at 353 nm. The quenching constant obtained from the least square fit (solid line), $\alpha = (3.61 \pm 0.55) \cdot 10^{-3}$ torr^{-1} may be compared with that given previously, $\alpha = 3.5 \cdot 10^{-3}$ torr^{-1}. At the lower temperature of 220 K the quantum yields at atmospheric pressure at 340 and 353 nm are markedly lower, as Figures 15 and 16 show. A similar Stern-Volume plot for ϕ(CO) at 353 nm is shown in Figure 17b. The least square fit results in a higher quenching constant of $\alpha = (10.8 \pm 2.6)10^{-3}$ torr^{-1}. Thus, the quenching constant depends on temperature. Partially, the temperature dependence arises because lowering the temperature increases the number density of the gas mixture at constant pressure. This effect can be taken into account by defining the quenching constant in terms of number density instead of pressure,

$$\alpha^n = (760 \times T / 2.68 \times 273) \alpha^P$$

which gives $\alpha^n = 1.12 \cdot 10^{-19}$ cm^3/molecule at 300 K and $\alpha^n = 2.47 \cdot 10^{-19}$ cm^3/molecule at 220 K. The influence of temperature on the quenching probably enters on account of vibrational and rotational excitation of the formaldehyde molecule which becomes enhanced with higher temperatures and favors the dissociation channel competing with the quenching process.

Finally, the quantum yield ϕ_1 for the process $CH_2O + h\nu \longrightarrow H + HCO$ can be obtained from the relation $\phi_1 = \phi(CO)(1-R)$ where R is the $\phi(H_2)/\phi_{CO}$ ratio. Similarily, the quantum yield ϕ_2 for process $H_2CO + h\nu = H_2 + CO$ is derived from $\phi_2 = \phi(CO) \cdot R$. We assume that $\phi(CO) = 1$ between 295 and 327 nm. The results are shown in Figures 18 and 19 .

Photodissociation Coefficients

The photodisssociation coefficient for formaldehyde is defined as the integral

$$J(z,X) = \int_{\Delta\lambda} \phi(\lambda,z)\sigma(\lambda,z)F(\lambda,z,X)\, d\lambda$$

where ϕ is the quantum yield, σ the absorption cross section, and F the solar photon flux, all as functions of the wavelength and altitude z. The solar flux is in addition dependent on the zenith angle X. The absorption cross sections may be taken as independent of z since the experimental data indicate an almost negligible effect of temperature and pressure. The quantum yields are fairly independent of temperature at wavelengths less than 330 nm. At wavelengths above 330 nm there is a dependence on temperature but a much greater independence on pressure which must be taken into account. Here, the quantum yield can be assumed to obey the Stern Volmer equation

$$\phi(\lambda,p) = 1/(1+\alpha(\lambda)p)$$

where p is the pressure and $\alpha(\lambda)$ is the quenching constant. If $\phi_A(\lambda)$ is the quantum yield of CO at atmospheric pressure, the quenching constant is given by

$$\alpha(\lambda) = \frac{1}{p_A} \quad \frac{1 - \phi_A(\lambda)}{\phi_A(\lambda)}$$

and $\phi_T(\lambda)$ can be approximated from the experimental data as

$$\phi_A(\lambda) = 1 - \beta \frac{\lambda - \lambda_o}{\lambda_1 - \lambda_o}$$

where λ_o = 329 nm, $\lambda_1 - \lambda_o$ = 355-329 = 26 nm and $\beta = 1 - \phi_A(355)$ = 0.74 as measured. The temperature effect of quenching was not yet taken into account in this calculation. The CO quantum yield in the spectral region 329-360 nm is then given by

$$\phi(CO) = \phi(\lambda,p) = 1/\left[1 + (p/p_A)(1 - \phi_A(\lambda))/\phi_A(\lambda)\right]$$

The two basic routes of formaldehyde photodecomposition in air are

(1) $HCHO + h\nu \longrightarrow H + HCO \xrightarrow{O_2} 2\,HO_2 + CO$

$\longrightarrow H_2 + Co$

The associated quantum yields are ϕ_1 and ϕ_2. From the experimental data they are given by

$$\phi_1 = \phi(CO) - \phi(H_2) = \phi(CO)(1-R(\lambda))$$

$$\phi_2 = \phi(H_2) = \phi(CO)\ R(\lambda)$$

$$\text{with } R(\lambda) = \phi(H_2)/\phi(CO)$$

The calculation of the corresponding photodissociation coefficients J_1 and J_2 made use of $R(\lambda)$ in conjunction with the CO quantum yield given above. The quantum yields used in the calculations are given in Table 5. They are close but not identical with the quantum yields which resulted from the final evaluation of experimental data which were deduced from Figures 14 and 15 and are also presented in Table 5. The photodissociation coefficients calculated with the preliminary data are not expected to change singnificantly when the more recent quantum yields are incorporated.

The assumption of attenuation of the solar flux in the Earth's atmosphere solely by absorption leads to the generalized Beer's law

$$F(\lambda,z,X) = F_0(\lambda)\exp(-\sec X\int_z^\infty \sum \sigma(\lambda)n_i(z)dz$$

where $F_0(\lambda)$ is the incident flux, X the zenith angle and the summation must include all important absorbers of index i with number densities $n_i(z)$ as a function of altitude. At wavelengths above 240 nm the major absorbers are ozone and nitrogen dioxide. Their number densities and absorption cross sections were taken from Luther and Gelinas (1976). With increasing penetration into the atmosphere, the direct solar radiation suffers Rayleigh scattering (to some extent also particulate scattering which is neglected here). Scattering diminishes the direct radiation flux, but at the same time it gives rise to a second contribution $F_{Sc}(z)$ to the total radiation field which reaches the point of consideration from all directions, so that $F_{Sc}(z)$ represents an integral over the scattered radiation from all angles. Luther and Gelinas (1976) have made a complete study of the effect of scattering on the photodissociation coefficient of several molecules, using radiation transfer theory. Isaksen et al (1976) have used a simplified approach noting that scattering is more pronounced in the direction of incoming solar radiation than in all other directions, and they have taken half of the scattering to occur forwards, the other half backwards. For five orders of scattering, the results were found to agree substantially with

those obtained by Luther and Gelinas.

In the present program the approach of Isaksen et al (1976) was adopted. It allows for the assumption of a surface albedo, for which the value 0.3 was assumed. Solar flux data were taken from Ackerman (1974). The data are given for 37 wavelength intervals in the region 230-382.5 nm. The formaldehyde spectrum was subdivided into 429 equidistant wavelength intervals covering the wavelength range 240.8-361 nm. The cross section for each interval was folded with the corresponding quantum yields taken from Table 5, and the light flux computed for the coarser wavelength intervals according to Ackerman, and the sums of the individual terms were calculated. The calculating routine starts at 55 km and then moves downward kilometer by kilometer until it reaches ground level.

Calculated photodissociation coefficients are given in Table 6 and Figure 20 for three zenith angles: 30, 50 and 70 degrees. The increases of the photodissociation coefficients with altitude, apparent from Figure 20 are due to a combination of effects: (a) increasing light intensity, caused in the troposphere by an increasing contribution of backscattering, and in the stratosphere by the increasing availability of UV radiation below 300 nm; and (b) the pressure effect at wavelengths above 330 nm whereby the quantum yield increases as the pressure drops. The individual quantum yields for the two photolytic pathways are of similar size near ground level and at the top of the stratosphere. In the middle atmosphere J_2 is greater than J_1, because here the pressure effect in the long-wavelength domain increases the production of H_2 with altitude while the contribution of formaldehyde decomposition in the spectral region below 300 nm does not yet take hold.

It should be re-emphasized that the photodissociation coefficients given here must be considered preliminary. In the future, it will be necessary to incorporate the temperature effect at wavelengths greater than 330 nm when computing formaldehyde photodissociation coefficients. An appropriate investigation will be started as soon as our computing facility which has suffered a temporary breakdown is restored. The influence which the tempera-

ture might have on the quantum yields at wavelengths below 290 nm can then also be explored.

References:

1. Ackerman, M. (1977), Stratospheric pollution and related ultraviolet radiation phenomena, Aeronomic Acta A-181, Institut D'Aëronomie Spatial de Belgique.

2. Clark, J.H., C.B. Moore,and N.S. Nogar (1978), The Photochemistry of Formaldehyde: Absolute quantum yields, radical reactions, and NO reaction. J.Chem.Phys. 68, 1264-1271.

3. Horowitz, A., and J.G. Calvert (1978), Wavelength dependence of the quantum efficiencies of the primary processes in formaldehyde photolysis at 25°C.
Int.J.Chem. Kinet. 10, 805-819.

4. Isaksen, I.S.A., K. Midtbö, J. Sunde,and P.J. Crutzen (1977), A simplified method to include molecular scattering and reflection in calculations of photon fluxes and photodissociation rates.
Geophys. Norv. 31, 11-26.

5. Luther, F.M., and R.J. Gelinas (1976), Effect of molecular multiple scattering and surface albedo on atmospheric photodissociation rates.
J.Geophys.Res. 81, 1125-1132.

6. Moortgat, G.K., and P. Warneck (1979), CO and H_2 quantum yields in the photodecomposition of formaldehyde in air.
J.Chem.Phys. 70, 3639-3651.

List of Tables

List of Figures

Figure 19. Quantum yield for CH_2O photodecomposition process 2.

Figure 20. Photodissociation coefficients of CH_2O as a function of altitude and zenith angle.

Temp.: $-58,6 \pm 1\ ^{o}C$
$214,6 \pm 1\ ^{o}K$

Pressure: $1o,8 \pm o.7$ torr

Spectral Resolution : o.5 nm

Code Nr.	Wave-length (nm)	Band	6261CX	6262CX	6263CX	6264CX	$\bar{\sigma} \cdot 1o^{-2o}$
			$\sigma \cdot 1o^{-20}$				
1	353,36	4^1	2,64o	2,716	2,648	2,67o	2,669 ± o,o34
2	343,55	4^3	2,3o6	2,369	2,331	2,299	2,326 ± o,o32
3	339,1o	$2^1 4^1$	5,619	5,693	5,644	5,647	5,651 ± o,o31
4	33o,o8	$2^1 4^3$	4,883	4,922	4,882	4,863	4,888 ± o,o25
5	326,57	$2^2 4^1$	6,971	6,852	6,973	6,955	6,938 ± o,o58
6	321,45	$5^1/1^1 4^1$	1,874	1,836	1,781	1,795	1,822 ± o,o41
7	317,29	$2^2 4^3$	6,412	6,417	6,335	6,348	6,378 ± o,o43
8	314,66	$2^3 4^1$	7,219	7,282	7,182	7,227	7,228 ± o,o41
9	312,5o	$1^1 4^3$	1,[illegible]	1,576	1,51o	1,572	1,578 ± o,o58
1o	3o9,25	$2^1 5^1$	3,967	4,oo2	3,935	4,o19	3,985 ± o,o31
11	3o5,67	$2^3 4^3$	5,7o5	5,7o7	5,7o3	5,833	5,737 ± o,o64
12	3o4,oo	$2^4 4^1$	8,o63	8,1o1	8,oo3	8,121	8,o72 ± o,o52
13	3o1,41	$1^1 2^1 4^3$	2,2o9	2,186	2,138	2,22o	2,188 ± o,o36
14	298,51	$2^5 4^1 + 1^1 2^2 4^1$	4,912	4,975	4,874	4,976	4,934 ± o,o5o
15	293,98	$2^5 4^1 + 2^4 4^3$	8,653	8,782	8,7o8	8,743	8,722 ± o,o55
16	291,25	$1^1 2^2 4^3$	1.963	1,954	1,92o	1,942	1,945 ± o,o19
17	288,96	$2^3 5^1 + 1^1 2^3 4^1$	4,411	4,448	4,441	4,457	4,439 ± o,o2o
18	284,93	$2^6 4^1$	5,659	5,715	5,642	5,693	5,677 ± o,o33
19	282,o5	$1^2 2^3 4^3$	1,49o	1,5o9	1,486	1,5o7	1,498 ± o,o12
2o	28o,51	$2^4 5^1$	3,152	3,239	3,14o	3,155	3,172 ± o,o45
21	277,11	$2^6 4^3$	2,641	2,716	2,634	2,7o8	2,674 ± o,o43
22	276,17	$2^7 4^1$	2,679	2,773	2,673	2,755	2,72o ± o,o51
23	272,o9	$2^5 5^1 + 1^1 2^4 4^3$	1,889	1,953	1,896	1,94o	1,919 ± o,o33
24	269,28	$2^7 4^3$	1,175	1,243	1,181	1,222	1,2o5 ± o,o33
25	268,11	$2^8 4^1$	1,383	1,435	1,4o2	1,456	1,419 ± o,o33
26	264,17	$2^6 5^1$	1,o27	1,o9o	1,o26	1,o84	1,o57 ± o,o35

T °K	211,2	214,6	26o,3	264,6	277,5	3o2,5
T °C	-62	-58,6	-12,9	-8,6	4,3	29,3
p Torr	12,1±o,3	1o,8±o,7	1o,6±o,5	1o,6±o,5	11,1±o,4	1o,8±o,5
Code Nr.	613CX	626,1-4CX	6271CX	6265aCX	5314CX	6123CX
	$\sigma.1o^{-2o}$	$\sigma.1o^{-2o}$	$\sigma.1o^{-2o}$	$\sigma.1o^{-2o}$	$\sigma.1o^{-2o}$	$\sigma.1o^{-2o}$
1	2,739	2,669	2,519	2,647	2,49o	2,4o7
2	2,381	2,326	2,152	2,3o6	2,22o	2,157
3	5,678	5,651	5,535	5,575	5,49o	5,388
4	4,856	4,888	4,721	4,835	4,82o	4,617
5	6,972	6,983	6,951	7,o91	7,o1o	6,9o5
6	1,796	1,822	1,775	1,819	1,7oo	1,726
7	6,258	6,378	6,169	6,318	6,48o	6,485
8	7,129	7,228	7,o56	7,158	7,18o	6,753
9	1,414	1,578	1,292	1,533	1,63o	1.521
1o	3,854	3,985	3,589	3,84o	3,87o	3,688
11	5,644	5,737	5,463	5,721	5,32o	5,687
12	7,777	8,o72	7,655	7,871	7,73o	7,574
13	2,o21	2,188	1,955	2,28o	2,2oo	2,o29
14	4,786	4,934	4,533	4,758	4,76o	4,534
15	8,585	8,722	7,859	8,o4o	8,o3o	7,561
16	1,863	1,945	1,735	1,9o9	1,81o	1,896
17	4,28o	4,439	3,972	4,186	3,99o	4,o63
18	5,593	5,677	5,o67	5,294	5,o2o	5,o43
19	1,391	1,498	1,322	1,458	1,5o4	1,539
2o	3,1o3	3,172	2,831	2,917	2,89o	2,864
21	2,6o4	2,674	2,434	2,542	2,524	2,477
22	2,643	2,72o	2,368	2,432	2,463	2,37o
23	1,851	1,919	1,76o	1,766	1,815	1,773
24	1,111	1,2o5	1,o8o	1,o51	1,114	1,118
25	1,332	1,419	1,2o8	1,24o	1,278	1,278
26	o,999	1,o57	o,976	o,952	o,986	o,983

Spectral resolution: o,5 nm

Table 2 (continued)

t[°C]	3o,5		2o,3		28,1		26,7		3o.5	
Code Nr.	6124CX		6123CX		6122CX		6121CX		6125CX	
λ	[Torr]σ.1o^{-2o}		[Torr]σ.1o^{-2o}		[Torr]σ.1o^{-2o}		[Torr]σ.1o^{-2o}		[Torr]σ.1o^{-2o}	
1	7,78	2,486	11,21	2,4o7	15,13	2,423	17.92	2,415	3,58	2,185
2	7,78	2,169	11,o7	2,157	15,o8	2,121	17,82	2,172	3;57	1,[illegible]
3	7,78	5,549	11,o2	5,388	15,o3	5,284	17,72	5,268	3,555	4,[illegible]
4	7,78	4,777	1o,97	4,[illegible]	14,98	4,762	17,63	4,589	3,52	4,26o
5	7,83	7,[illegible]	1o,92	[illegible],9o5	14,93	6,778	17,58	6,511	3,51	6,416
6	7,88	1,[illegible]	1o,87	[illegible],726	14,89	1,762	17,43	1,699	3,5o	1,445
7	7,93	6,96o	1o,77	6,485	14,89	6,314	17,38	6,195	3,5o	6,126
8	7,93	7,335	1o,77	6,753	14,89	7,829	17,33	6,77o	3,48	6,664
9	7,98	1,48o	1o,72	1,521	14,84	1,589	17,33	1,498	3,48	1,395
1o	7,98	3,776	1o,72	3,688	14,79	3,781	17,29	3,7o3	3,48	3,226
11	8,o3	5,7o1	1o,72	5,687	14,74	5,788	17,24	5,795	3,48	4,725
12	8,o3	7,875	1o,67	7,574	14,74	7,611	17,24	7,56o	3,48	6,599
13	8,o3	2,129	1o,67	2,o29	14,69	2,177	17,19	2,11o	3,47	1,665
14	8,o3	4,529	1o,63	4,534	14,69	4,614	17,14	4,591	3,47	4,o71
15	8,o3	7,569	1o,63	7,561	14,64	7,732	17,o9	7,673	3,45	6,43o
16	8,o3	1,831	1o,58	1,896	14,64	1,944	17,o4	1,923	3,44	1,764
17	8,o3	3,96o	1o,53	4,o63	14,64	4,163	16,99	4,1o5	3,44	3,559
18	8,o3	4,962	1o,53	5,143	14,59	5,158	16,89	5,167	3,43	4,296
19	8,o3	1,525	1o,48	1,5o1	14,54	1,582	16,84	1,695	3,43	1,457
2o	7,98	2,723	1o,48	2,864	14,54	2,936	16,84	2,952	3,43	2,492
21	7,98	2,4o6	1o,43	2,477	14,49	2,634	16,79	2,565	3,42	2,16o
22	7,98	2,269	1o,38	2,37o	14,49	2,535	16,79	2,5o5	3,42	2,139
23	7,93	1,736	1o,38	1,773	14,44	1,9o6	16,7o	1,872	3,41	1,721
24	7,93	1,142	1o,33	1,118	14,44	1.17o	16,65	1,164	3,41	1,1o5
25	7,93	1,251	1o,33	1,278	14,39	1,334	16,65	1,3o6	3,4o	1,236
26	7,88	o,984	1o,28	o,983	14,39	1,o64	16,6o	1,o34	3,4o	o,98o

Spectral Resolution : o.5 nm

Table 2 (continued)

T °K	316,6	328,0	341,3	353,1	362,2
T °C	41,4	54,8	68,1	8o,o	89,o
p Torr	11,1±o,4	1o,7±o,3	1o,8±o,3	1o,8±o,3	1o,6±o,3
Code Nr.	6212CX $\sigma.1o^{-2o}$	6213CX $\sigma.1o^{-2o}$	6214CX $\sigma.1o^{-2o}$	6215CX $\sigma.1o^{-2o}$	6216CX $\sigma.1o^{-2o}$
1	2,39o	2,225	2,329	2,3o4	2,295
2	1,94o	1,97o	2,o78	1,997	2,116
3	4,9oo	5,116	5,232	5,o53	5,375
4	4,432	4,6o6	4,6c6	4,571	4,86o
5	6,498	6,523	6,756	6,555	6,891
6	1,6o7	1,715	1,776	1,763	1,862
7	5,543	6,13o	6,289	6,169	6,538
8	6,561	6,677	6,911	6,712	7,o85
9	1,419	1,423	1,633	1,572	1,579
1o	3,463	3,5o3	3,683	3,537	3,742
11	5,384	5,594	5,832	5,345	6,o49
12	7,1o6	7,366	7,518	7,264	7,638
13	2,o7o	2,o63	2,164	2,1o2	2,3oo
14	4,173	4,272	4,425	4,244	4,658
15	7,1o4	7,216	7,3o2	7,o94	7,461
16	2,o36	1,85o	1,993	1,977	2,1o2
17	3,783	3,882	4,o4o	3,884	4,o81
18	4,686	4,774	4,831	4,749	4,9o5
19	1,539	1,562	1,6o2	1,586	1,731
2o	2,736	2,789	2,863	2,814	2,874
21	2,347	2,478	2,53o	2,444	2,568
22	2,271	2,299	2,438	2,283	2,4o2
23	1,718	1,769	1,833	1,744	1,848
24	1,o7o	1,1o3	1,15o	1,142	1,154
25	1,25o	1,26o	1,297	1,238	1,355
26	o,971	1,o5o	1,o64	1,o26	1,o79

Table 3

Absorption cross sections of H_2CO at 5 nm resolution : measurement at 22o K are compared with data obtained at 298 K. The data are extrapollated at zero pressure.

λ nm	220 K	298 K
353.1	1.11×10^{-20}	0.96×10^{-20}
339.3	2.3o	2.4o
327.o	3.37	3.6o
315.2	4.6o	4.52
3o4.4	4.24	4.44
294.9	3.64	3.48
285.6	2.9o	2.46
278.1	1.97	1.6o
27o.6	1.14	1.oo
262.o	o.66	o.62
253	o.3o	o.27
244	o.1o	o.1o

Table 4 A. Experimental conditions and quantum yields at 300 K.

λ nm	P torr	CH_2O ppmv	I_o 10_3^{14} ph/ cm^2.sec	I_{abs} 10^{11} ph/ sec	t sec	H_2 ppbv	CO ppbv	$\frac{H_2}{CO}$	ϕ_{H_2}	ϕ_{CO}
253.0	735	99.3	0.590	0.095	15612	92.6	158.5	0.584	0.483	0.826
	652	136.0	0.581	0.114	8832	81.7	137.6	0.523	0.491	0.939
	703	129.3	0.414	0.083	5130	29.3	48.3	0.606	0.508	0.838
	692	125.9	0.452	0.087	9846	50.0	79.2	0.632	0.426	0.674
	757	107.2	0.443	0.079	11913	69.8	96.7	0.722	0.588	0.814
							Average	0.613	0.483	0.818
							±	0.073	0.071	0.095
262.0	699	96.0	1.209	0.412	1095	337.5	571.3	0.591	0.551	0.932
	659	145.3	0.947	0.460	1088	303.4	509.2	0.596	0.420	0.705
	682	117.7	0.725	0.295	8292	183.2	285.7	0.641	0.538	0.839
	622	111.0	0.757	0.265	8172	155.6	240.3	0.647	0.470	0.726
							Average	0.619	0.495	0.801
							±	0.029	0.061	0.106
270.6	714	102.7	1.742	1.045	6888	535.4	923.4	0.580	0.559	0.964
	672	142.7	1.492	1.171	5298	372.1	711.2	0.523	0.420	0.802
	675	122.1	1.306	0.881	5796	317.7	563.2	0.564	0.442	0.784
	787	114.8	1.190	0.880	5964	309.5	567.0	0.546	0.489	0.896
							Average	0.553	0.477	0.862
							±	0.025	0.061	0.084
278.1	724	104.9	2.322	2.309	4128	465.3	1162.1	0.400	0.372	0.929
	667	116.2	1.553	1.576	4524	419.4	908.7	0.461	0.413	0.895
	776	111.0	1.443	1.627	6738	508.0	1196.8	0.424	0.380	0.895
							Average	0.429	0.388	0.906
							±	0.031	0.022	0.020
285.6	734	106.0	2.610	4.077	3744	583.9	1923.2	0.304	0.296	0.974
	766	164.0	2.115	5.347	6324	1193.8	4056.0	0.294	0.326	0.967
	742	132.6	1.989	3.939	2406	395.9	1179.7	0.335	0.326	0.972
	767	105.1	1.712	2.779	3996	430.7	1415.7	0.304	0.313	1.029
							Average	0.309	0.315	0.985
							±	0.018	0.014	0.029

Table 4 A. Experimental conditions and quantum yields at 300 K.

λ nm	P torr	CH_2O ppmv	I_o 10_3^{14} ph/ cm².sec	I_{abs} 10^{11} ph/ sec	t sec	H_2 ppbv	CO ppbv	$\frac{H_2}{CO}$	ϕ_{H_2}	ϕ_{CO}
294.9	705	104.7	3.275	6.885	3732	962.6	3562.1	0.270	0.278	1.029
	752	131.4	2.325	6.543	1734	407.2	1519.5	0.268	0.284	1.060
	718	120.1	2.022	4.967	1728	355.5	1344.9	0.264	0.290	1.099
	648	117.1	2.182	4.713	3180	642.5	2374.0	0.271	0.293	1.080
	754	166.1	2.725	9.716	3936	1392.0	5242.8	0.266	0.290	1.088
							Average	0.268	0.287	1.071
							±	0.003	0.006	0.028
304.4	739	158.7	2.869	12.227	2784	981.1	4592.4	0.214	0.224	1.049
	723	130.2	2.836	9.704	2196	564.5	2818.2	0.200	0.212	1.006
	658	118.3	2.207	6.243	2850	615.6	2606.4	0.236	0.226	0.957
	781	106.8	1.200	4.853	4806	683.7	2903.6	0.235	0.258	1.097
	765	144.5	1.258	5.055	4572	562.5	2429.1	0.232	0.210	0.907
							Average	0.223	0.226	1.003
							±	0.016	0.019	0.075
315.3	750	166.9	2.819	12.617	2865	1146.3	4702.3	0.244	0.242	0.993
	753	128.4	1.187	4.247	4755	705.2	2539.2	0.278	0.297	1.068
	616	138.1	1.343	4.166	3075	574.5	2075.2	0.277	0.311	1.126
	250	58.6	1.345	0.730	9660	790.0	3049.8	0.259	0.316	1.220
							Average	0.264	0.292	1.101
							±	0.016	0.034	0.096
327.0	715	160.2	3.617	12.207	3082	2592.7	4375.5	0.593	0.519	0.875
	753	115.8	1.403	3.606	4668	1220.3	1908.4	0.639	0.616	0.963
	461	107.4	1.500	2.189	4052	999.4	1648.1	0.606	0.586	0.966
	633	140.3	1.506	3.943	3408	1385.8	2111.6	0.656	0.736	1.122
	213	50.3	1.509	0.477	3924	553.6	941.2	0.588	0.711	1.208
							Average	0.616	0.634	1.027
							±	0.030	0.090	0.135
339.3	699	160.0	5.268	11.572	3888	3460.6	3387.9	0.979	0.554	0.566
	640	140.6	2.021	2.411	6444	2037.6	2085.8	0.977	0.547	0.560
							Average	0.978	0.550	0.563
							±	0.002	0.005	0.004

Table 4 A. Experimental conditions and quantum yields at 300 K.

λ nm	P torr	CH_2O ppmv	I_o 10_3^{14} ph/ cm^2.sec	I_{abs} 10^{11} ph/ sec	t sec	H_2 ppbv	CO ppbv	$\frac{H_2}{CO}$	ϕ_{H_2}	ϕ_{CO}
353.1	478	105.3	3.082	1.333	6963	501.6	510.0	0.983	0.297	0.302
	189	39.0	3.284	2.039	5460	302.0	273.5	1.110	0.581	0.524
	301	57.7	3.137	0.455	5601	402.1	397.6	1.033	0.546	0.529
	70	14.7	3.383	0.027	11841	291.0	296.4	0.982	0.711	0.724
	113	24.7	3.381	0.074	11526	--	358.5	--	--	0.534
	653	152.9	2.920	2.292	10377	667.8	798.7	0.836	0.207	0.247
	585	137.2	2.571	1.621	7728	372.7	453.3	0.931	0.222	0.239
	301	71.2	2.746	0.462	8217	517.0	548.3	0.943	0.546	0.579
	180	42.5	2.800	0.168	11970	604.9	618.1	0.979	0.609	0.622
	255	57.6	2.926	0.338	10788	629.4	709.1	0.888	0.497	0.560
							Average	0.965		
							±	0.080		

Table 4 B. Experimental conditions and quantum yields at 22o K.

λ nm	P torr	CH_2O ppmv	I_o $1o_3^{14}$ ph/ cm^3.sec	I_{abs} $1o^{11}$ ph/ sec	t sec	H_2 ppbv	CO ppbv	$\frac{H_2}{CO}$	ϕ_{H_2}	ϕ_{CO}
27o.6	712	18o.7	o.493	o.795	4953	162.4	276.7	o.587	o.467	o.757
	739	175.9	o.555	o.914	885o	221.8	483.3	o.459	o.31o	o.676
							Average	o.523	o.388	o.717
							±	o.o9o	o.111	o.o57
278.1	721	181.4	o.642	1.859	4986	295.6	659.1	o.448	o.356	o.794
	748	182.6	o.724	2.164	7884	386.5	112o.4	o.345	o.259	o.752
	29o	71.2	o.666	o.3o1	5616	96.2	243.2	o.395	o.252	o.638
							Average	o.396	o.283	o.728
							±	o.o52	o.o59	o.o81
285.6	728	168.o	o.963	3.9oo	3831	3o9.2	968.o	o.319	o.237	o.742
	73o	184.7	o.789	3.492	417o	363.2	1151.8	o.315	o.284	o.9oo
	76o	18o.9	o.866	3.776	6165	489.4	1797.9	o.272	o.241	o.885
	43o	1oo.7	o.85o	1.195	5484	3oo.8	1o36.7	o.29o	o.3o4	1.o49
							Average	o.229	o.266	o.894
							±	o.o22	o.o33	o.125
294.9	685	62.5	1.15o	2.o11	5331	297.2	1132.4	o.263	o.278	1.o59
	737	161.3	1.242	6.126	3714	434.2	1915.8	o.222	o.217	o.975
	741	188.5	o.956	5.477	3534	5o4.8	2o45.7	o.247	o.3oo	1.216
	771	188.5	1.o21	5.921	3681	495.1	2o69.9	o.239	o.265	1.1o6
	386	95.3	1.138	1.682	4359	367.1	1382.6	o.265	o.294	1.1o7
	685	161.5	1.o51	4.638	3o96	386.8	1667.7	o.232	o.279	1.2o2
							Average	o.245	o.272	1.111
							±	o.o17	o.o3o	o.o9o
3o4.4	7o4	83.8	1.358	3.853	6513	48o.o	2164.9	o.222	o.2o9	o.943
	747	166.5	1.419	8.549	429o	661.7	3674.4	o.2oo	o.236	1.178
	564	129.o	1.556	5.396	4866	643.4	3o75.6	o.2o9	o.214	1.o23
	261	58.6	1.551	1.145	5628	29o.6	1256.6	o.231	o.181	o.781
	35o	84.4	1.226	1.695	2931	234.6	1oo3.7	o.234	o.251	1.o76
	681	168.8	1.223	6.481	36oo	425.6	2555.7	o.189	o.186	o.986
							Average	o.213	o.998	o.213
							±	o.o16	o.134	o.o27

Table 4 B. Experimental conditions and quantum yields at 22o K.

λ nm	P torr	CH_2O ppmv	I_o $1o_3^{14}$ ph/ cm^3.sec	I_{abs} $1o^{11}$ ph/ sec	t sec	H_2 ppbv	CO ppbv	$\frac{H_2}{CO}$	ϕ_{H_2}	ϕ_{CO}
315.3	728	92.7	1.244	4.329	4983	516.2	1878.1	o.275	o.269	o.979
	713	82.o	1.362	4.1o8	4728	5o5.2	1844.8	o.275	o.288	1.o46
	758	174.o	1.494	1o.356	3348	782.2	3o69.8	o.255	o.269	1.o56
	25o	53.6	1.66o	1.15o	4185	385.1	125o.6	o.3o8	o.31o	1.oo6
	57o	131.9	1.655	6.436	5949	1o99.1	4243.o	o.259	o.253	o.978
	672	166.1	1.3o7	7.524	2742	375.4	1692.7	o.322	o.274	o.852
							Average	o.282	o.277	o.986
							±	o.o27	o.o2o	o.o73
327.o	668	12o.2	1.651	5.o57	3612	1o35.9	1549.9	o.668	o.591	o.884
	611	1oo.5	1.712	3.974	2922	915.5	1327.7	o.689	o.744	1.o79
	6o1	94.2	1.732	3.713	3699	1266.9	1579.3	o.8o2	o.858	1.o69
	779	185.8	1.664	9.269	3321	1436.4	2329.3	o.617	o.572	o.928
	65o	15o.2	1.57o	5.819	3939	1699.3	2488.5	o.683	o.748	1.o95
	351	72.9	1.849	1.787	4257	1o47.4	1457.2	o.719	o.746	1.o39
	25o	55.9	1.833	o.975	4143	791.5	1161.5	o.681	o.762	1.118
							Average	o.694	o.717	1.o3o
							±	o.o57	o.o1o	o.o89
339.3	657	12o.4	2.316	4.7o5	43o5	947.6	878.2	1.o79	o.473+	o.438+
	621	1o8.1	2.439	4.266	4572	1oo4.8	9o3.6	1.112	o.5oo+	o.449+
	679	149.3	1.9o8	5.o35	5817	1397.9	1248.9	1.119	o.5o6+	o.452+
	486	93.4	2.213	2.622	6957	1859.o	1567.4	1.164	o.724	o.623
	3o5	67.o	2.228	1.197	7752	1486.9	1246.2	1.193	o.769	o.645
	136	29.7	2.229	o.234	7884	1o75.4	882.o	1.219	1.249	1.o24
	3o7	73.3	2.o6o	1.172	6285	624.9	649.3	o.962	o.394	o.41o
	618	145.9	2.o65	4.678	462o	1299.7	1255.2	1.o34	o.559+	o.54o+
							Average	1.11o	o.5o9+	o.5o8+
							±	o.o85	o.o36	o.o95

+) Average for atmospheric pressure only.

Table 4 B. Experimental conditions and quantum yields at 22o K.

λ nm	P torr	CH_2O ppmv	I_o $1o_3^{14}$ ph/ cm^3.sec	I_{abs} $1o^{11}$ ph/ sec	t sec	H_2 ppbv	CO ppbv	$\frac{H_2}{CO}$	ϕ_{H_2}	ϕ_{CO}
353.1	648	12o.6	3.331	3.198	43o5	198.o	183.6	1.o78	o.143+	o.133+
	314	53.8	3.44o	o.727	4458	2o2.6	194.4	1.o42	o.3o5	o.292
	439	69.3	3.468	1.332	37o5	171.o	158.6	1.o78	o.238	o.221
	689	77.5	2.655	1.8o6	5232	143.7	137.o	1.o49	o.166+	o.158+
	214	45.4	2.683	o.329	8364	199.8	176.o	1.135	o.245	o.216
	689	156.2	2.694	3.634	6327	17o.o	178.3	o.953	o.o79+	o.o83+
	783	191.4	3.112	5.676	6882	317.4	276.9	1.146	o.o97+	o.o85+
	393	1oo.7	3.oo8	1.476	9537	367.4	352.2	1.o43	o.158	o.151
	252	61.6	1.92o	o.791	83o7	245.8	2o6.8	1.189	o.311	o.262
	61o	145.1	3.oo5	3.238	8361	358.1	363.7	o.985	o.122+	o.124+
	36o	82.5	2.967	1.o75	3531	42o.4	419.1	1.oo3	o.278	o.277
							Average	1.o7o	o.124+	o.117+
							±	o.o73	o.o38	o.o32

+) Average for atmospheric pressure only.

Table 5. Quantum yields

	Prosisional data used for the calculation of the J-values in Table 6		Final data obtained from evaluation of recent results shown in Fig. 14 and 15.	
λ (nm)	ϕ_{CO}	$R = \frac{H_2}{CO}$	ϕ_{CO}	$R = \frac{H_2}{CO}$
240	0.690	0.710	0.630	0.670
245	0.730	0.685	0.670	0.665
250	0.770	0.670	0.705	0.655
255	0.805	0.640	0.745	0.638
260	0.840	0.620	0.780	0.618
265	0.875	0.580	0.820	0.586
270	0.910	0.540	0.860	0.533
275	0.935	0.470	0.895	0.457
280	0.960	0.415	0.934	0.370
285	0.985	0.350	0.963	0.310
290	0.995	0.290	0.980	0.270
292	1.000	0.284	0.987	0.260
294	1.000	0.268	0.992	0.248
296	1.000	0.254	0.996	0.237
298	1.000	0.236	1.000	0.227
300	1.000	0.230	1.000	0.220
302	1.000	0.214	1.000	0.218
304	1.000	0.198	1.000	0.217
306	1.000	0.188	1.000	0.218
308	1.000	0.184	1.000	0.222
310	1.000	0.180	1.000	0.230
312	1.000	0.184	1.000	0.240
314	1.000	0.200	1.000	0.260
316	1.000	0.230	1.000	0.285
318	1.000	0.265	1.000	0.322
320	1.000	0.315	1.000	0.380
322	1.000	0.375	1.000	0.448
324	1.000	0.445	1.000	0.522
326	1.000	0.520	1.000	0.613

Table 5 (continued)

λ (nm)	ϕ_{CO}	$R = \frac{H_2}{CO}$	ϕ_{CO}	$R = \frac{H_2}{CO}$
328	1.000	0.585	1.000	0.720
330	F	0.640	F	0.825
332	F	0.683	F	0.912
334	F	0.726	F	0.958
336	F	0.761	F	0.982
338	F	0.786	F	0.995
340	F	0.812	F	1.000
342	F	0.882	F	1.000
344	F	0.836	F	1.000
346	F	0.843	F	1.000
348	F	0.854	F	1.000
350	F	0.865	F	1.000
352	F	0.869	F	1.000
354	F	0.871	F	1.000
356	F	0.875	F	1.000
358	F	0.878	F	1.000
360	F	0.882	F	1.000

F :At wavelengths larger than 329 nm, the ϕ_{CO} can be calculated from the following expression:

$$\phi_{CO}(\lambda,p) = \frac{1}{1 + \frac{p}{p_A} \cdot \frac{1 - \phi_A}{\phi_A}}$$

where $\phi_A = 1 - \beta \frac{\lambda - \lambda_0}{\lambda_1 - \lambda_0}$

$p_A = 760$ torr

and $\beta = 0.74$

$\lambda_0 = 329$ nm

$\lambda_1 = 355$ nm

Table 6. Formaldehyde photodissociation Coefficients (in 10^{-5} s^{-1})

z	p	T	$\chi = 30^{o}$			$\chi = 50^{o}$			$\chi = 70^{o}$		
(km)	(mb)	(K)	J_1	J_2	J_{tot}	J_1	J_2	J_{tot}	J_1	J_2	J_{tot}
0	1013.2	288.1	2.122	2.498	4.619	1.751	2.266	4.017	0.801	1.467	2.347
1	898.7	281.6	2.952	3.491	6.444	2.449	3.187	5.636	1.273	2.132	3.405
2	795.0	275.1	3.146	3.742	6.889	2.624	3.435	6.059	1.408	2.371	3.779
4	616.6	262.2	3.520	4.313	7.771	2.963	3.940	6.903	1.681	2.876	4.558
6	472.2	249.2	3.873	4.766	8.639	3.284	4.456	7.740	1.956	3.413	5.369
8	356.5	236.2	4.201	5.285	9.486	3.585	4.978	8.563	2.226	3.972	6.198
10	265.0	223.2	4.502	5.799	10.301	3.864	5.497	9.361	2.486	4.543	7.030
12	194.0	216.6	4.773	6.291	11.065	4.115	5.997	10.112	2.728	5.104	7.832
14	141.7	216.6	4.992	6.714	11.705	4.319	6.425	10.715	2.928	5.589	8.518
16	103.5	216.6	5.173	7.064	12.237	4.489	6.782	11.272	3.095	5.995	9.090
18	75.6	216.6	5.334	7.355	12.689	4.643	7.079	11.721	3.245	6.332	9.577
20	55.3	216.6	5.497	7.597	13.095	4.799	7.327	12.126	3.395	6.615	10.011
22	40.5	218.6	5.682	7.805	13.487	4.979	7.540	12.520	3.566	6.860	10.426
24	29.7	220.6	5.909	7.989	13.898	5.204	7.731	12.936	3.778	7.079	10.857
26	21.9	222.5	6.187	8.161	14.348	5.486	7.910	13.396	4.047	7.285	11.332
28	16.2	224.5	6.512	8.324	14.836	5.819	8.081	13.900	4.376	7.482	11.858
30	12.0	226.5	6.878	8.483	15.361	6.199	8.247	14.447	4.765	7.673	12.438
32	8.89	228.5	7.292	8.644	15.936	6.633	8.715	15.048	5.225	7.866	13.091
34	6.63	233.7	7.754	8.813	16.567	7.122	8.590	15.713	5.758	8.064	13.823
36	5.06	239.3	8.249	8.989	17.239	7.652	8.774	16.427	6.351	8.268	14.619
38	3.81	244.8	8.767	9.179	17.946	8.217	8.971	17.189	7.001	8.484	15.486
40	2.87	250.3	9.288	9.381	18.670	8.798	9.184	17.982	7.698	8.719	16.416

Table 6. continued

z (km)	p (mb)	T (K)	X = 30°			X = 50°			X = 70°		
			J_1	J_2	J_{tot}	J_1	J_2	J_{tot}	J_1	J_2	J_{tot}
42	2.22	255.9	9.763	9.586	19.350	9.341	9.401	18.742	8.972	9.240	18.212
44	1.72	261.4	10.133	9.770	19.904	9.777	9.602	19.380	8.971	9.193	18.164
46	1.33	266.6	10.382	9.910	20.291	10.080	9.762	19.843	9.407	9.390	18.798
48	1.03	270.4	10.537	10.005	20.542	10.276	9.877	20.153	9.710	9.547	19.257
50	0.798	270.6	10.638	10.070	20.708	10.407	9.958	20.365	9.925	9.671	19.596
52	0.627	270.3	10.706	10.115	20.821	10.496	10.016	20.511	10.079	9.765	19.844
54	0.490	267.4	10.751	10.145	20.897	10.556	10.056	20.612	10.187	9.835	20.022

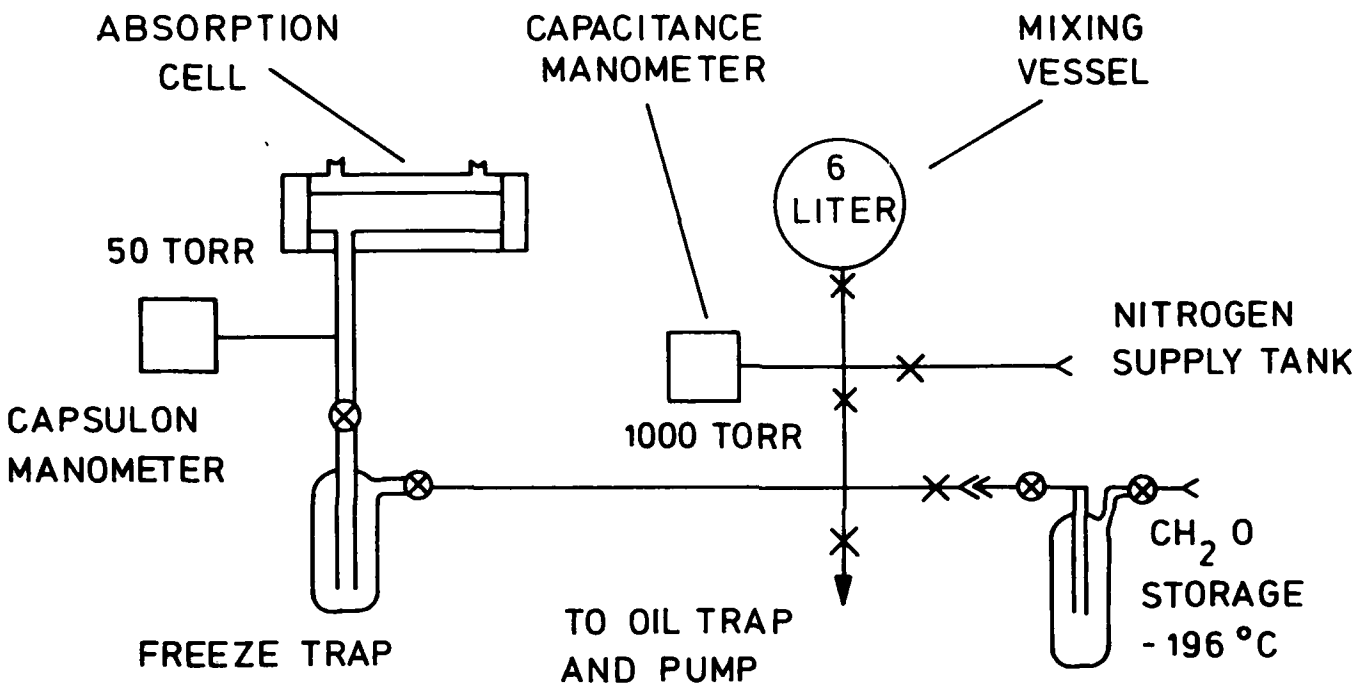

Figure 1. Gas handling manifold for the measurement of formaldehyde absorption cross sections.

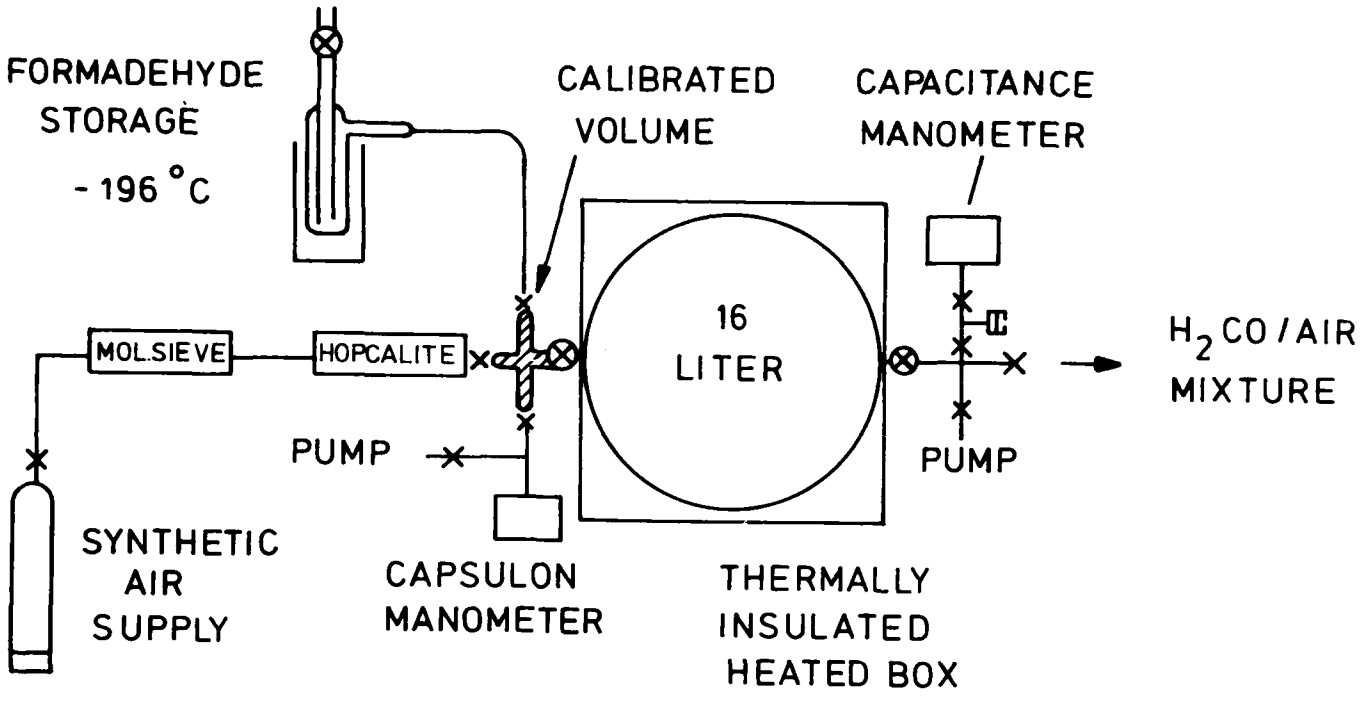

Figure 2. Preparation and storage of formaldehyde/air mixtures.

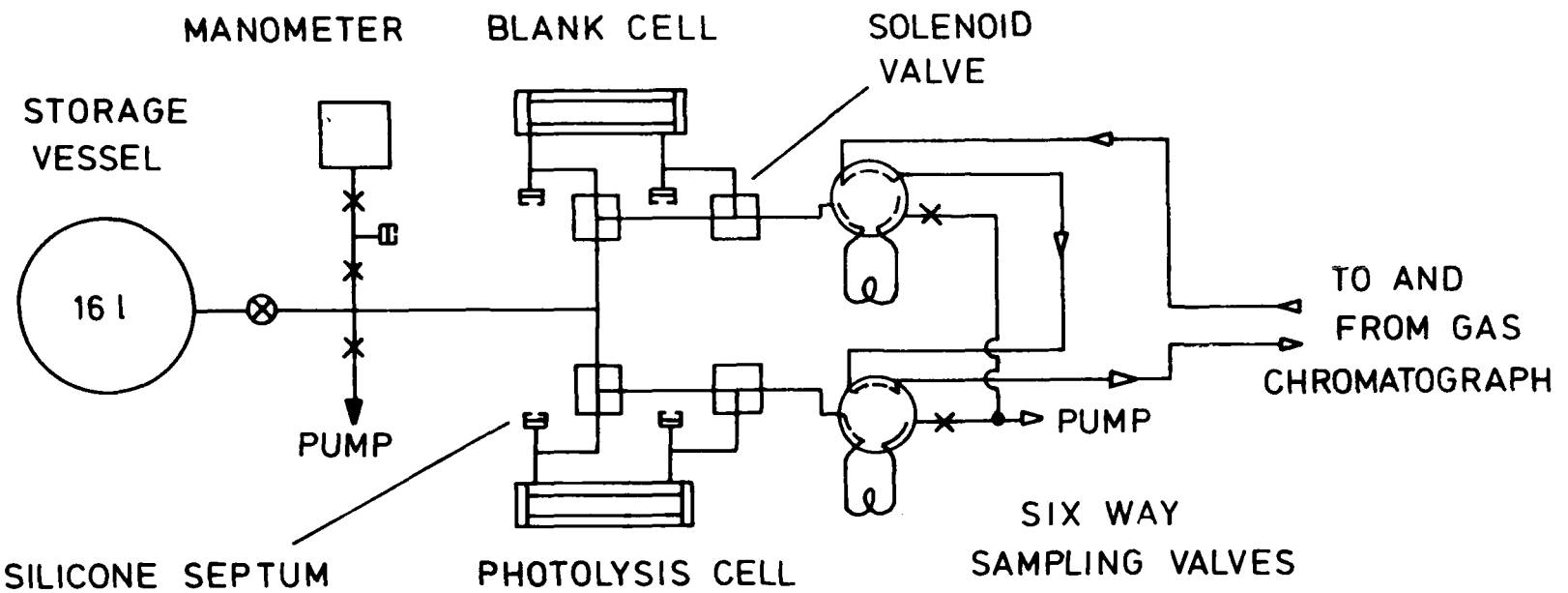

Figure 3. Arrangement for filling the photolysis cells and the withdrawal of samples for analysis.

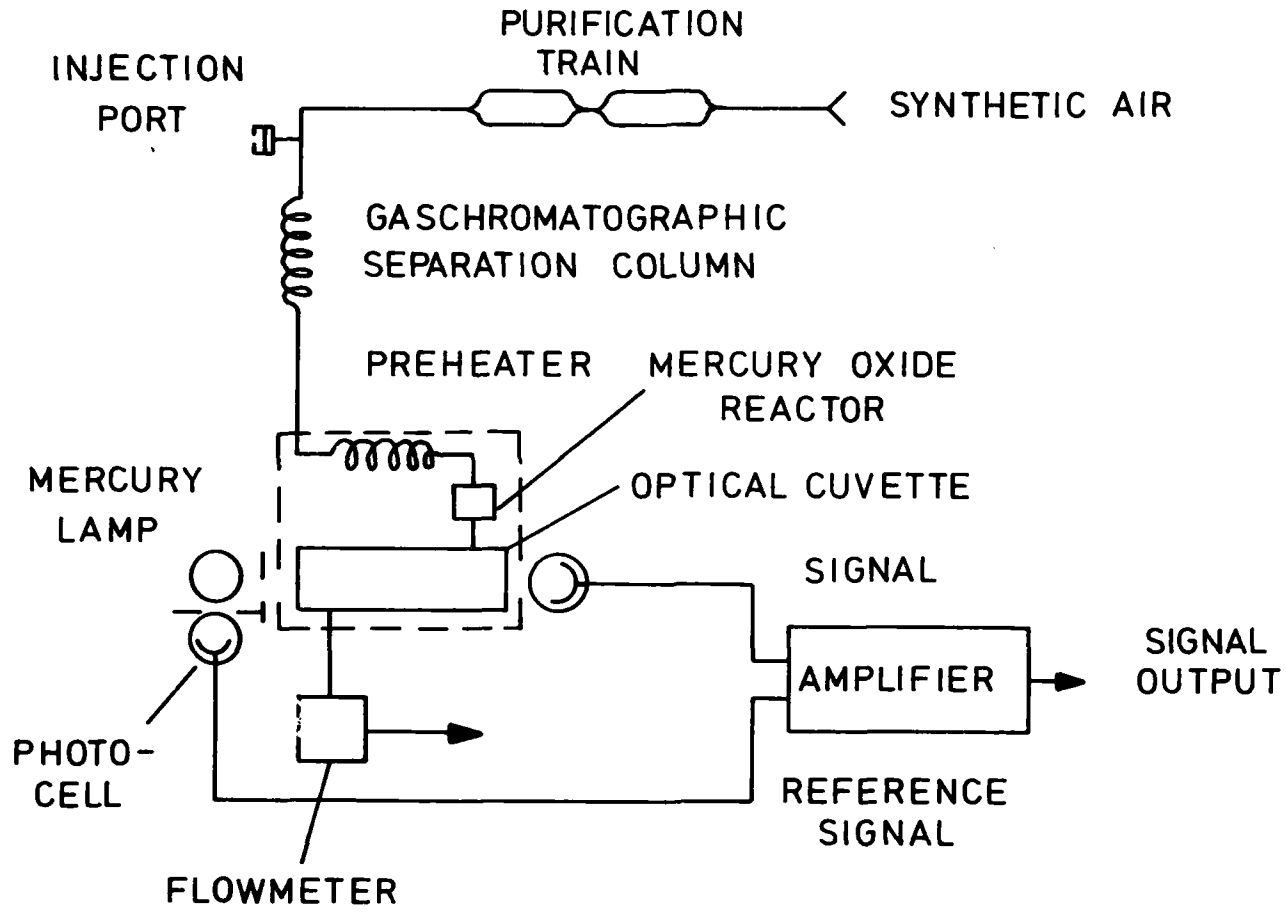

Figure 4. Schematic of the CU/H_2 analyser.

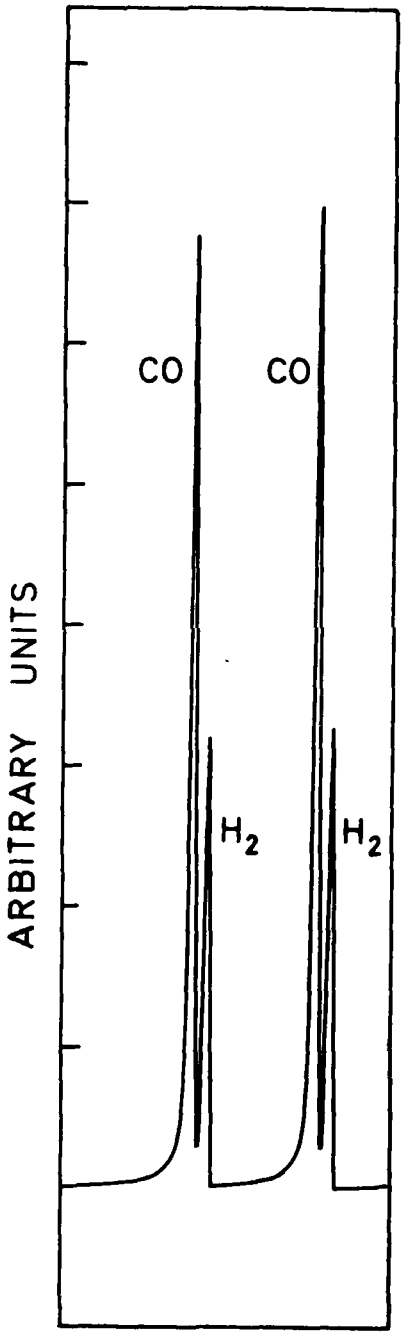

Figure 5. Example for the output obtained with the CO / H_2 analyser

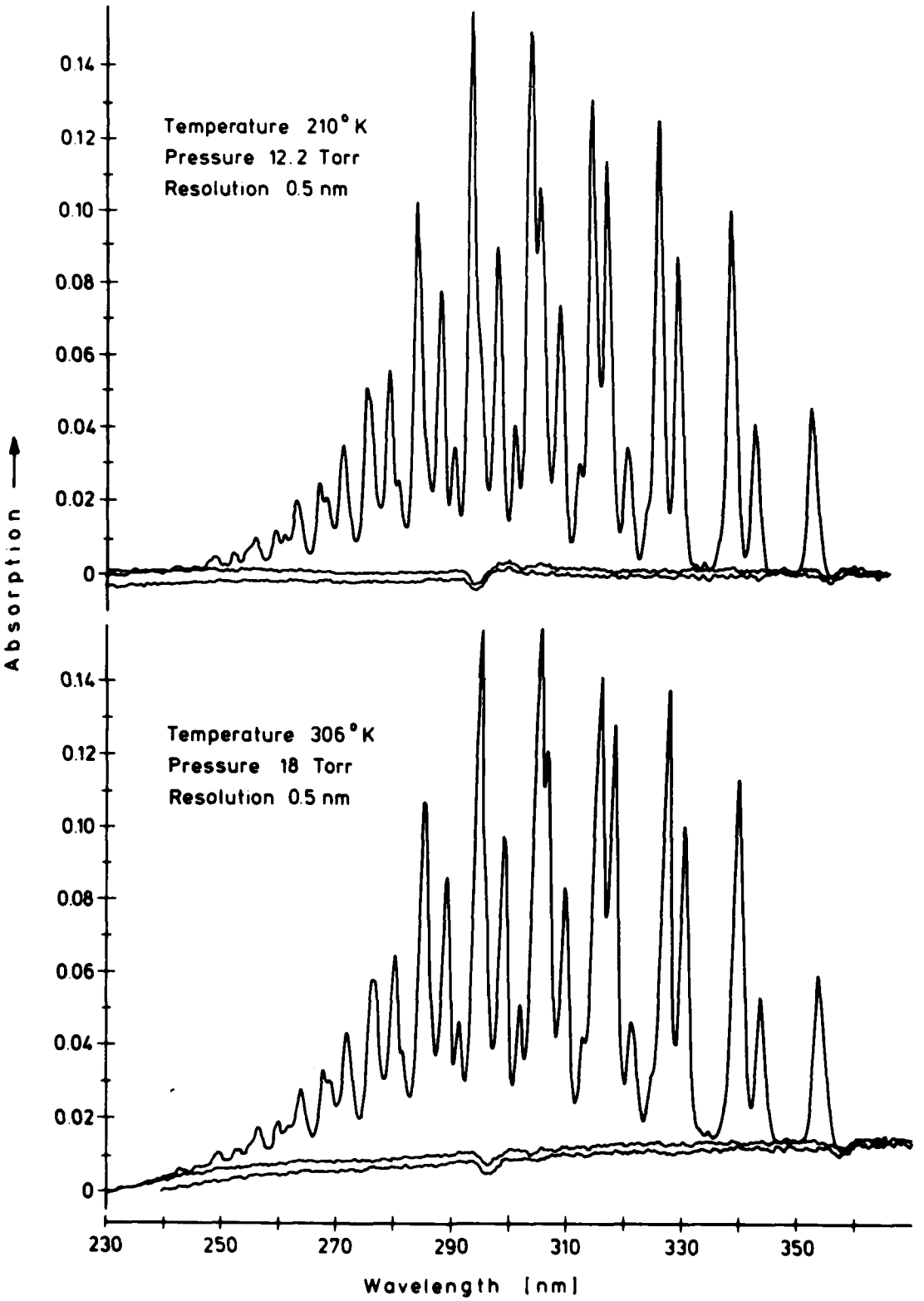

Figure 6. Comparison of near uv spectra of formaldehyde at temperatures of 306 and 210 K.

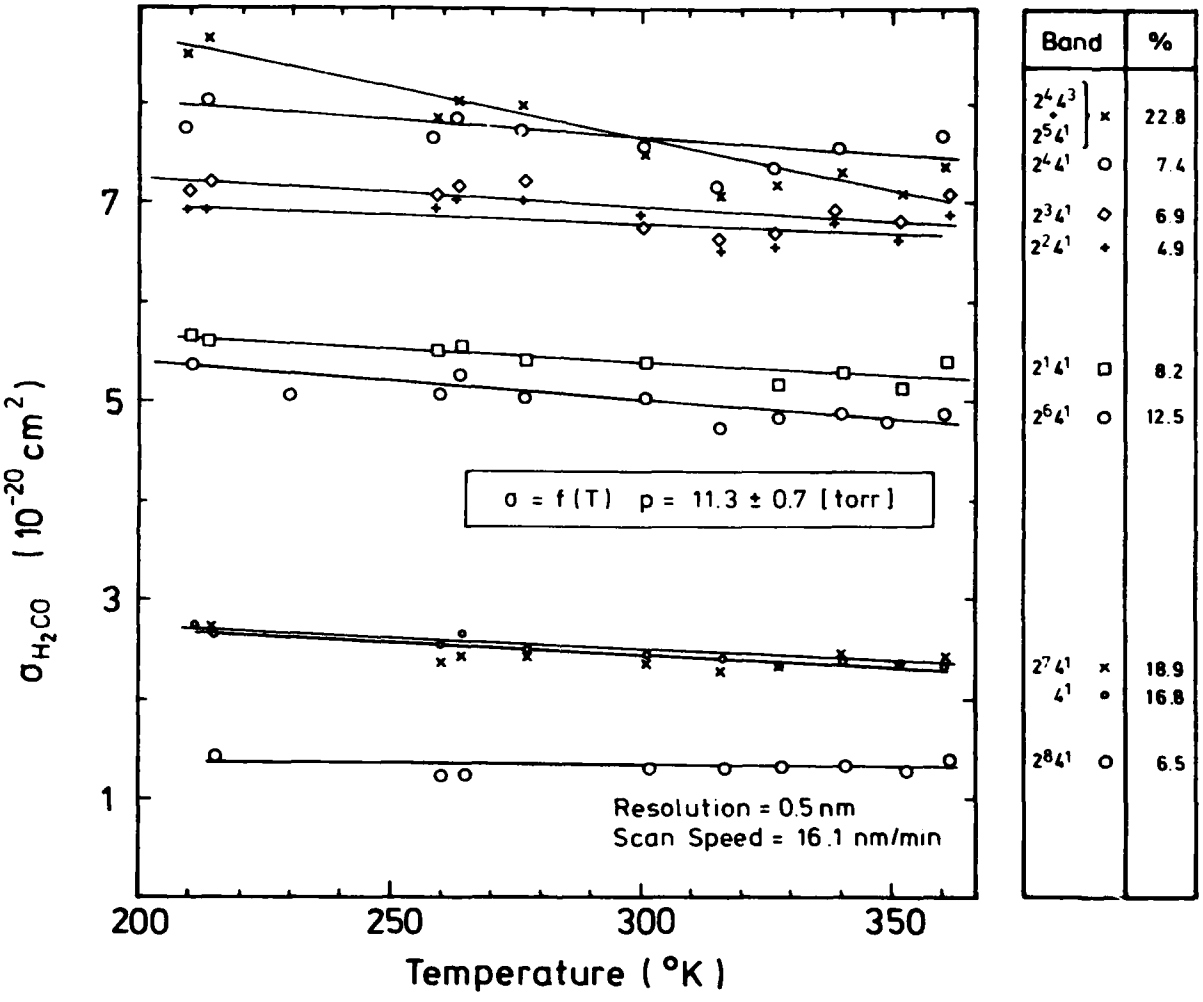

Figure 7. Plot of absorption cross sections of the CH_2O band maxima versus temperature. The percentage change is indicated on the right hand side for each band.

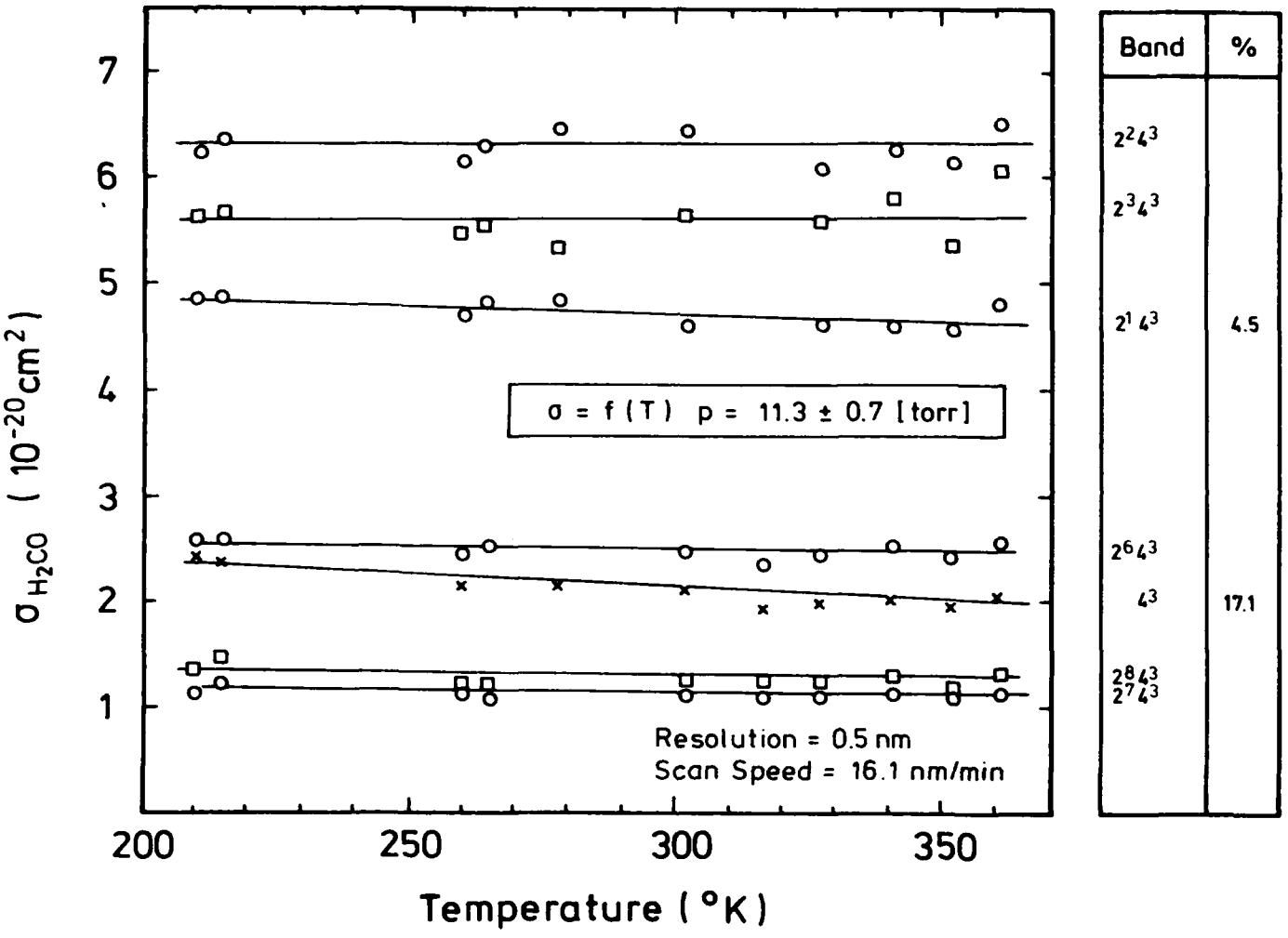

Figure 8. Plot of absorption cross sections of the CH_2O band maxima versus temperature. The percentage of change is indicated on the right hand side for each band.

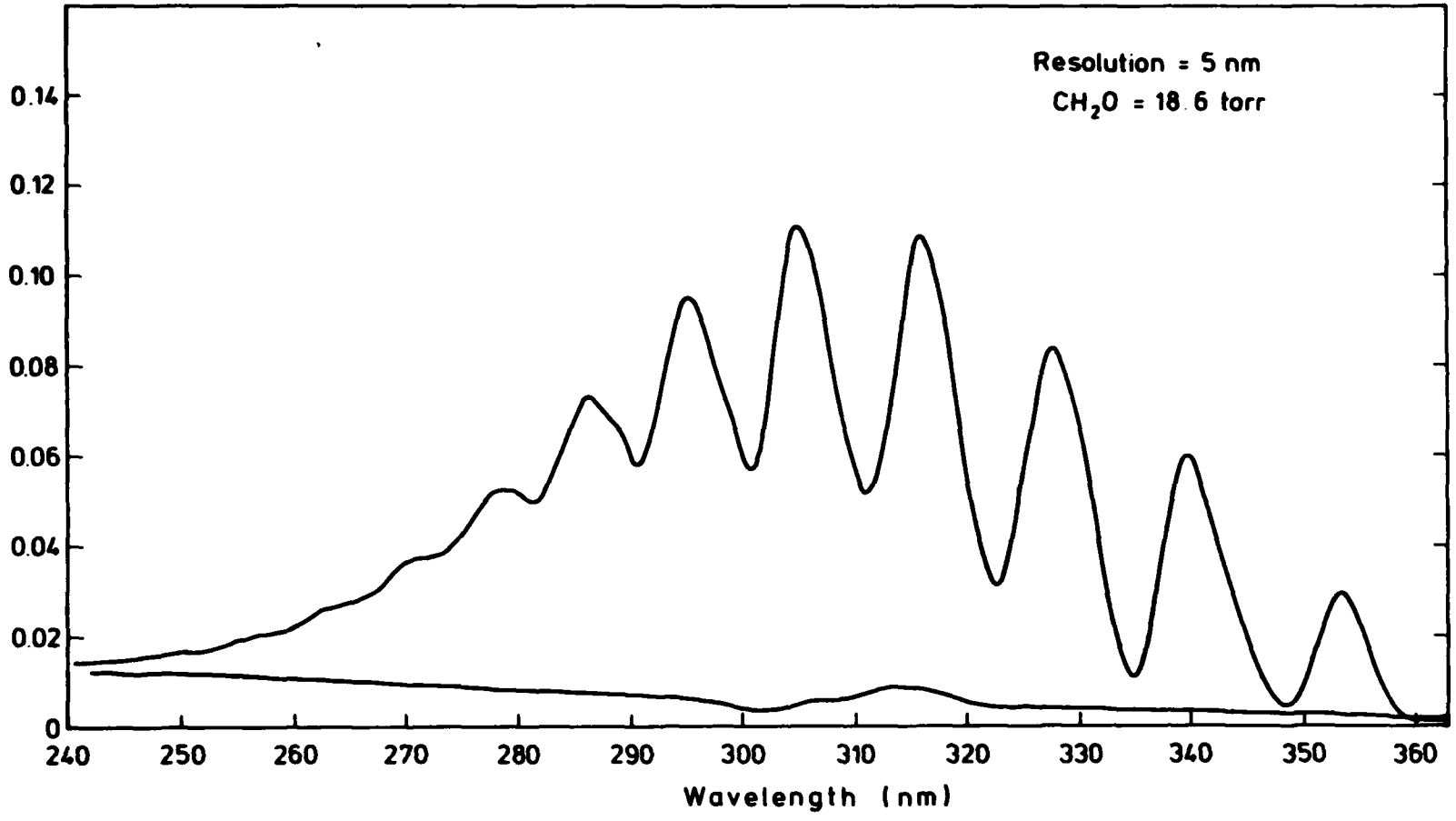

Figure 9. Low resolution spectrum of CH_2O.

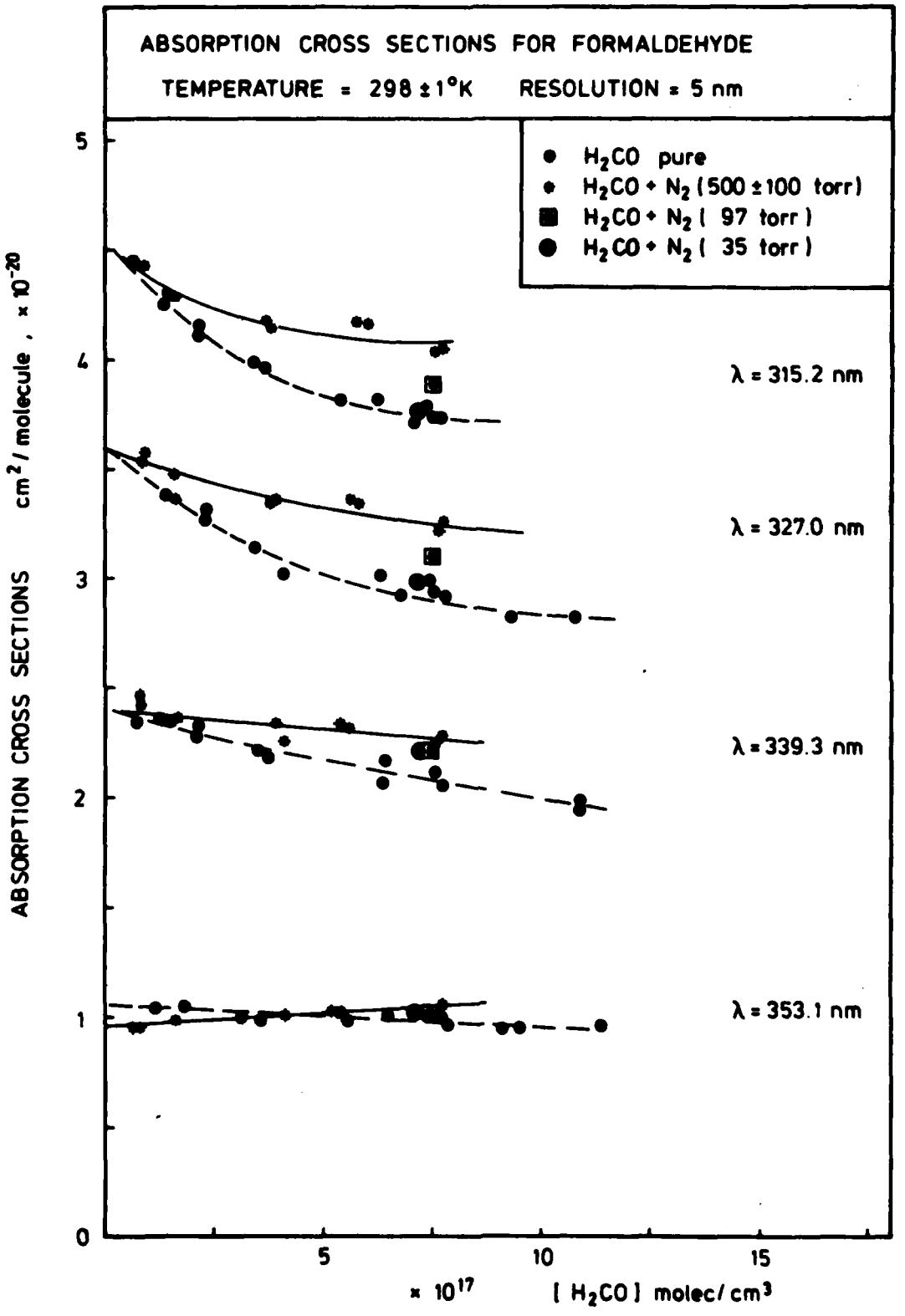

Figure 1o. CH_2O Absorption cross sections at 5nm spectral resolution for T = 298 K as a function of pressure.

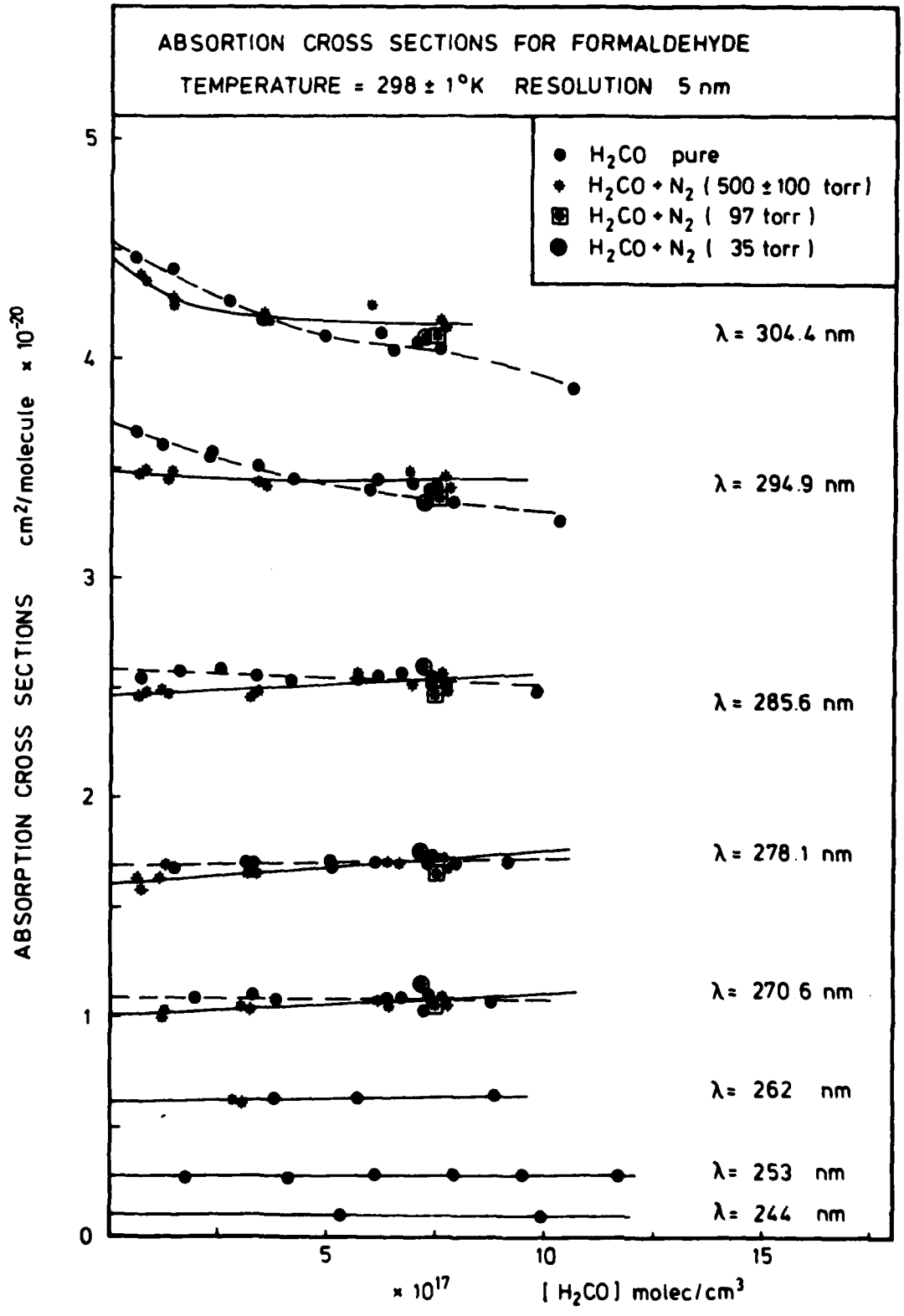

Figure 11. CH_2O Absorption cross sections at 5 nm spectral resolution for T = 298 K as a function of pressure.

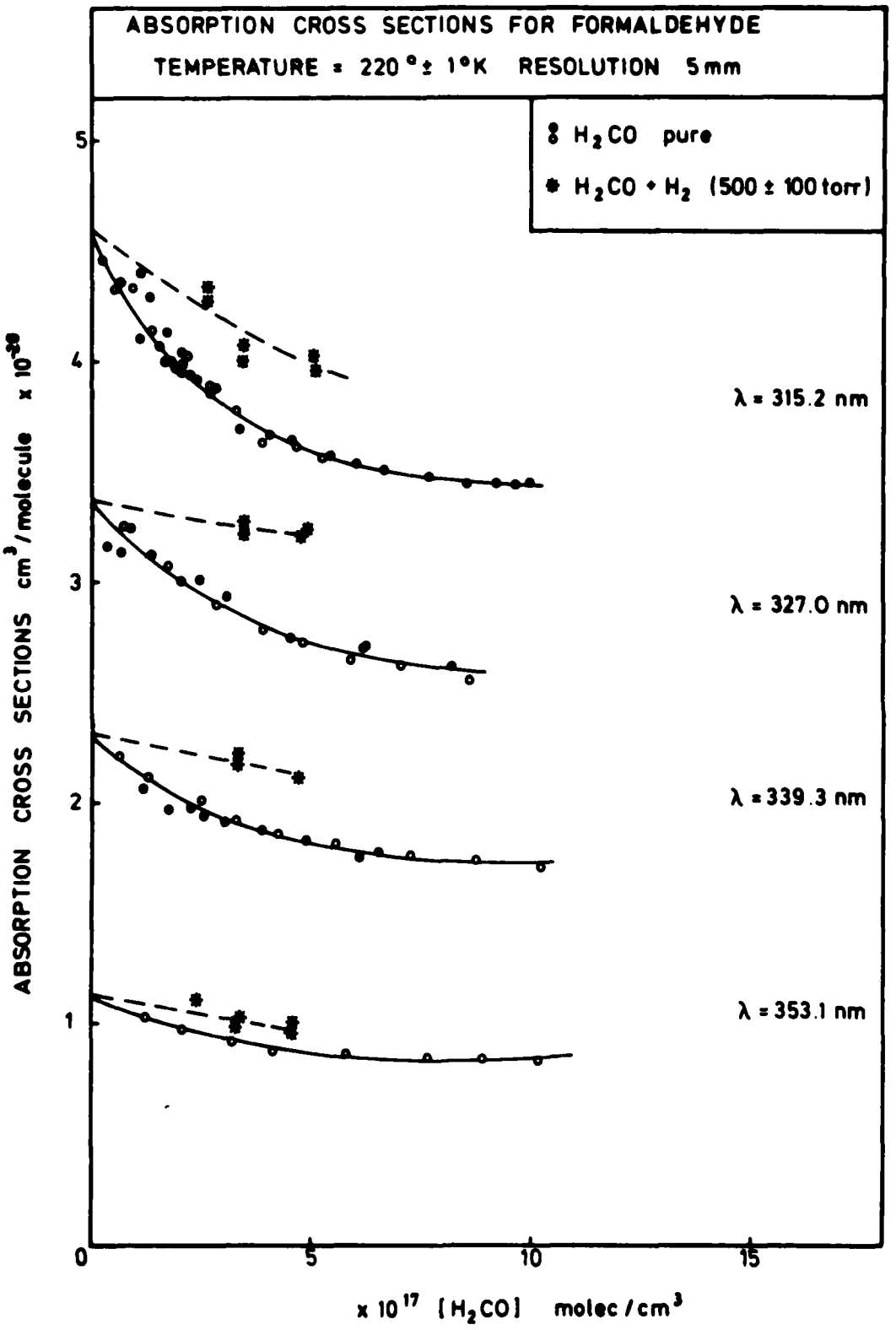

Figure 12. CH_2O Absorption cross sections at 5 nm spectral resolution for T = 220 K as a function of pressure.

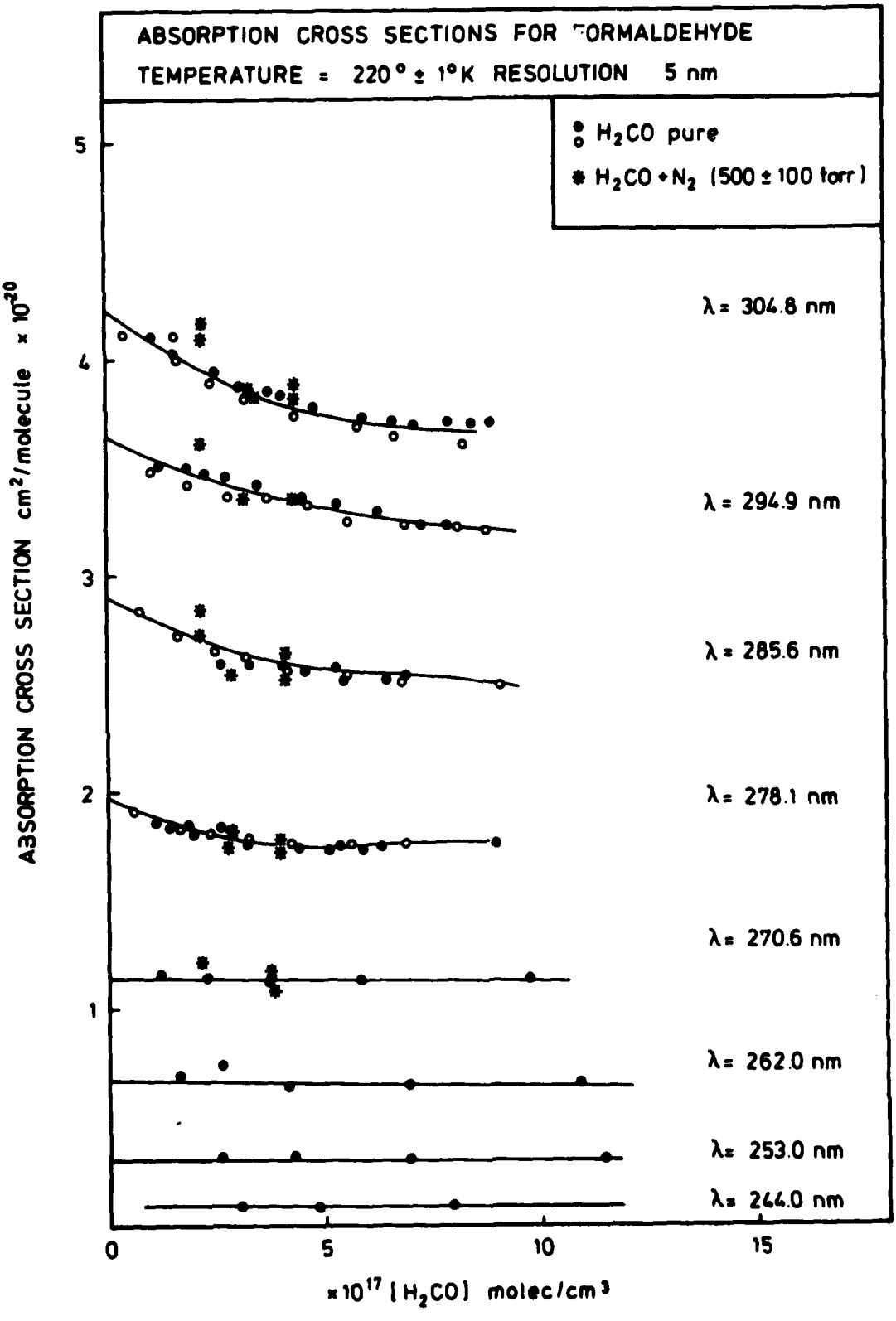

Figure 13. CH_2O Absorption cross sections at 5 nm spectral resolution for T = 220 K as a function of pressure.

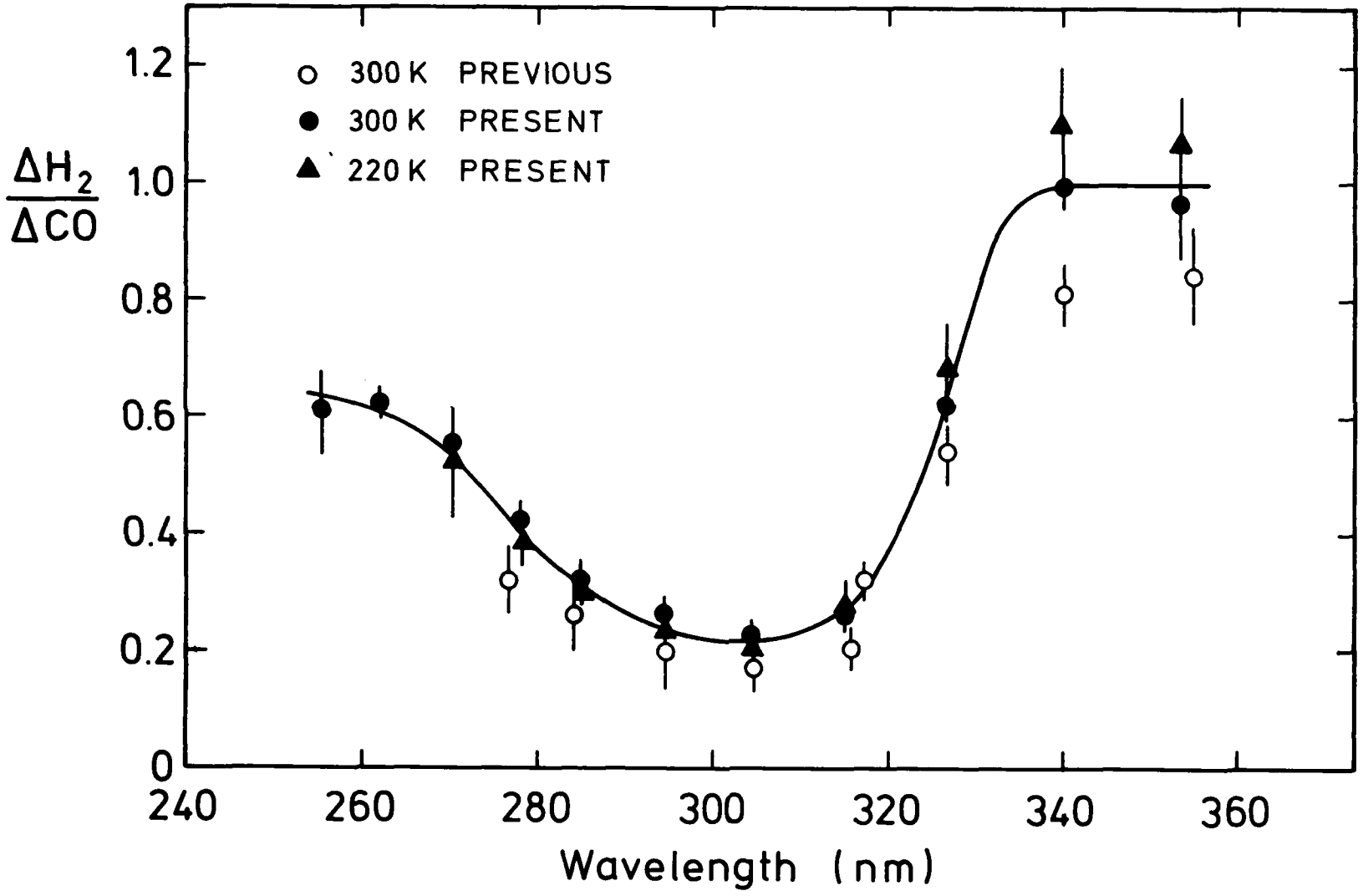

Figure 14. Ratio of H_2 and CO quantum yields in the photolysis of CH_2O versus wavelength.

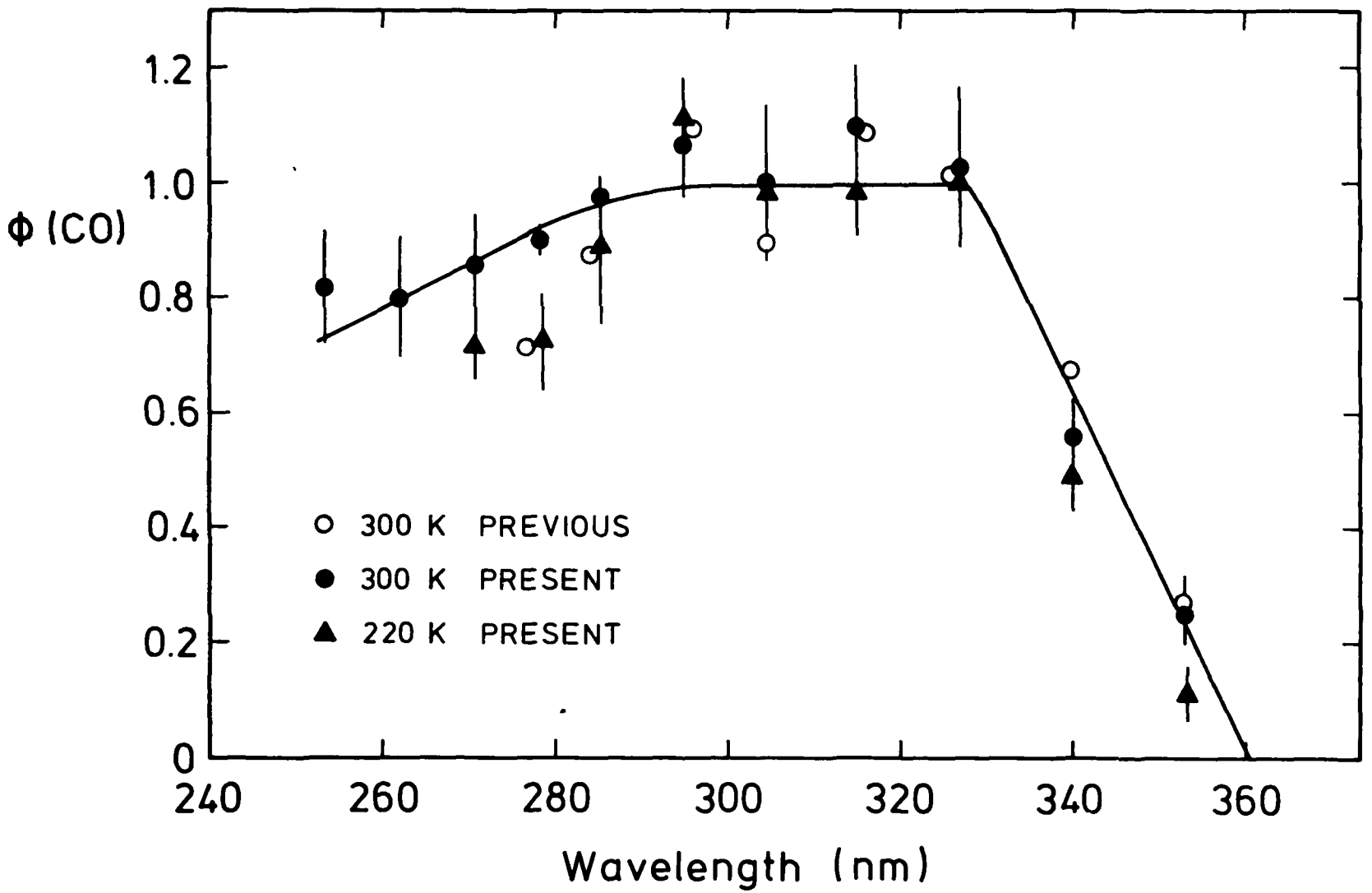

Figure 15. CO quantum yields as a function of wavelength.

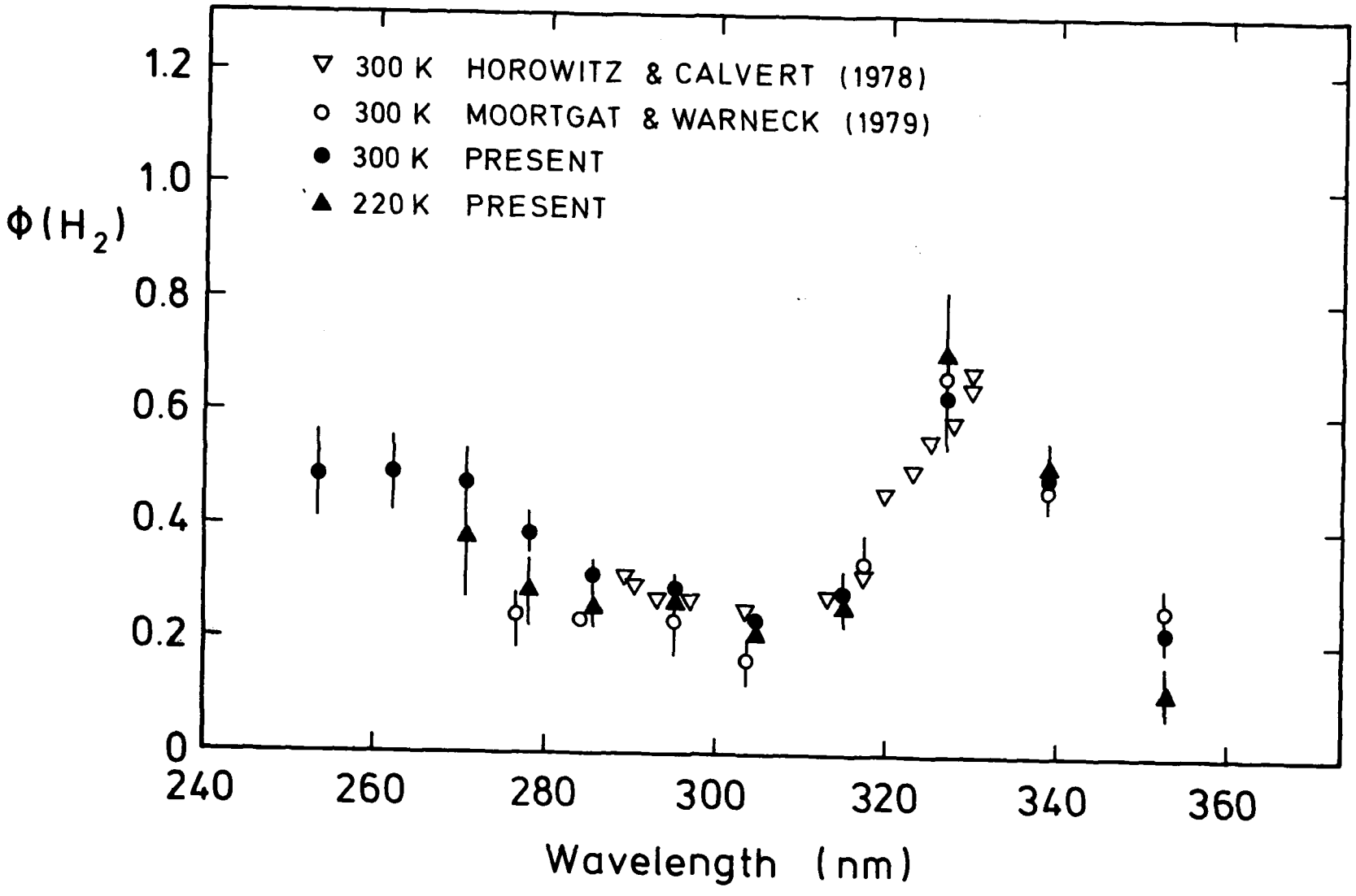

Figure 16. H_2 quantum yields as a function of wavelength.

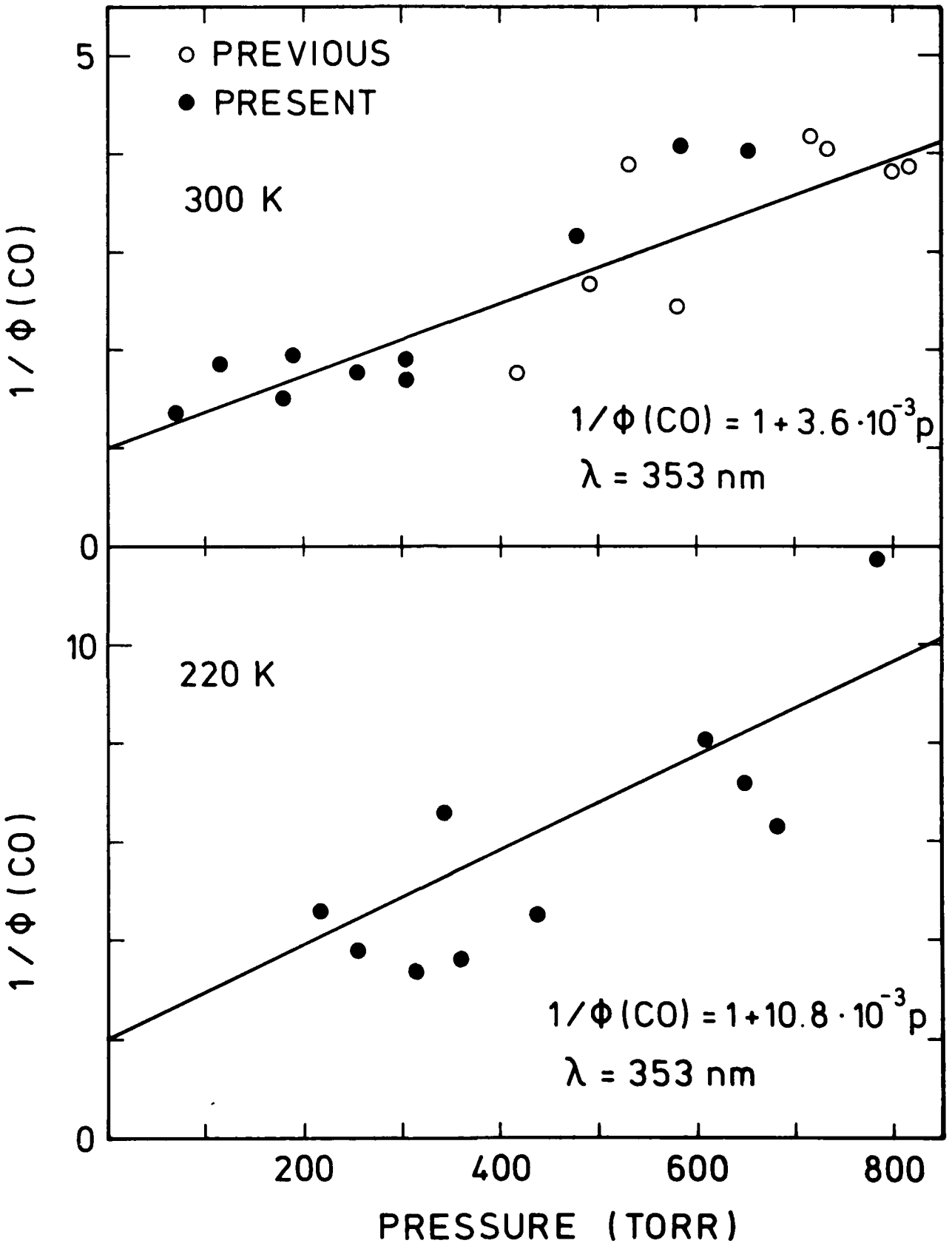

Figure 17. Stern-Volmer plots of CO quantum yields versus pressure
a) T = 300 K, b) T = 220 K.

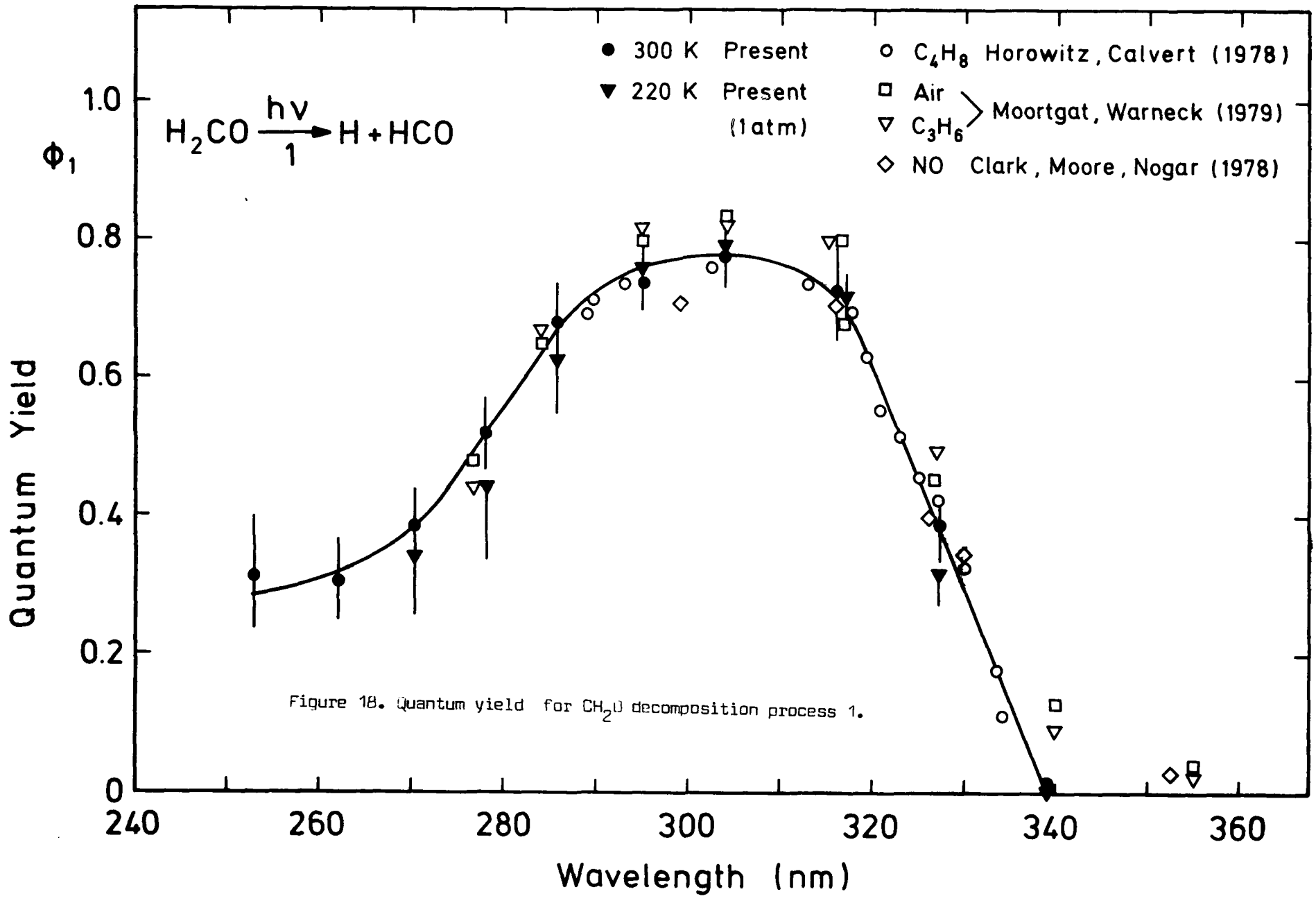

Figure 18. Quantum yield for CH_2O decomposition process 1.

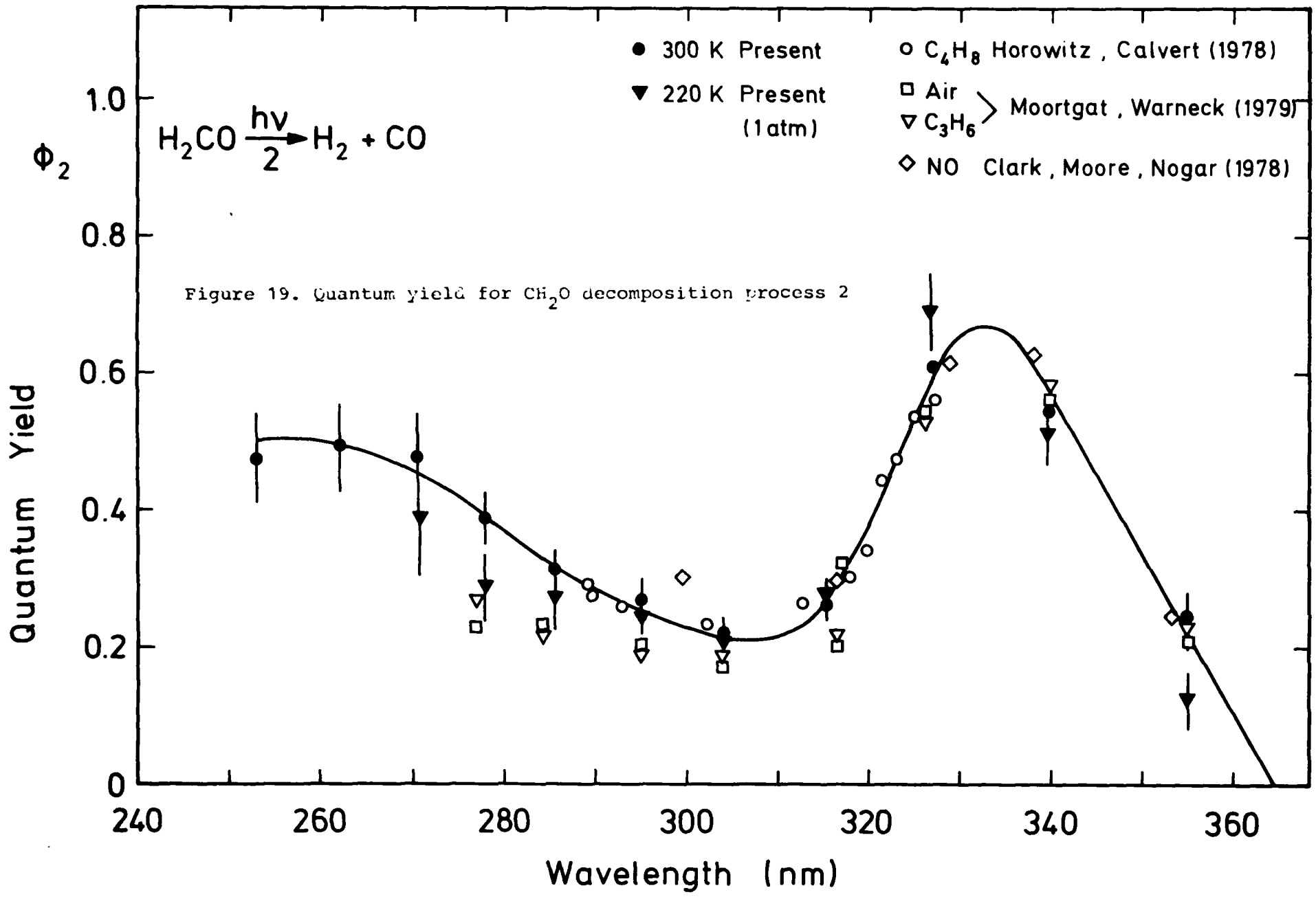

Figure 19. Quantum yield for CH_2O decomposition process 2

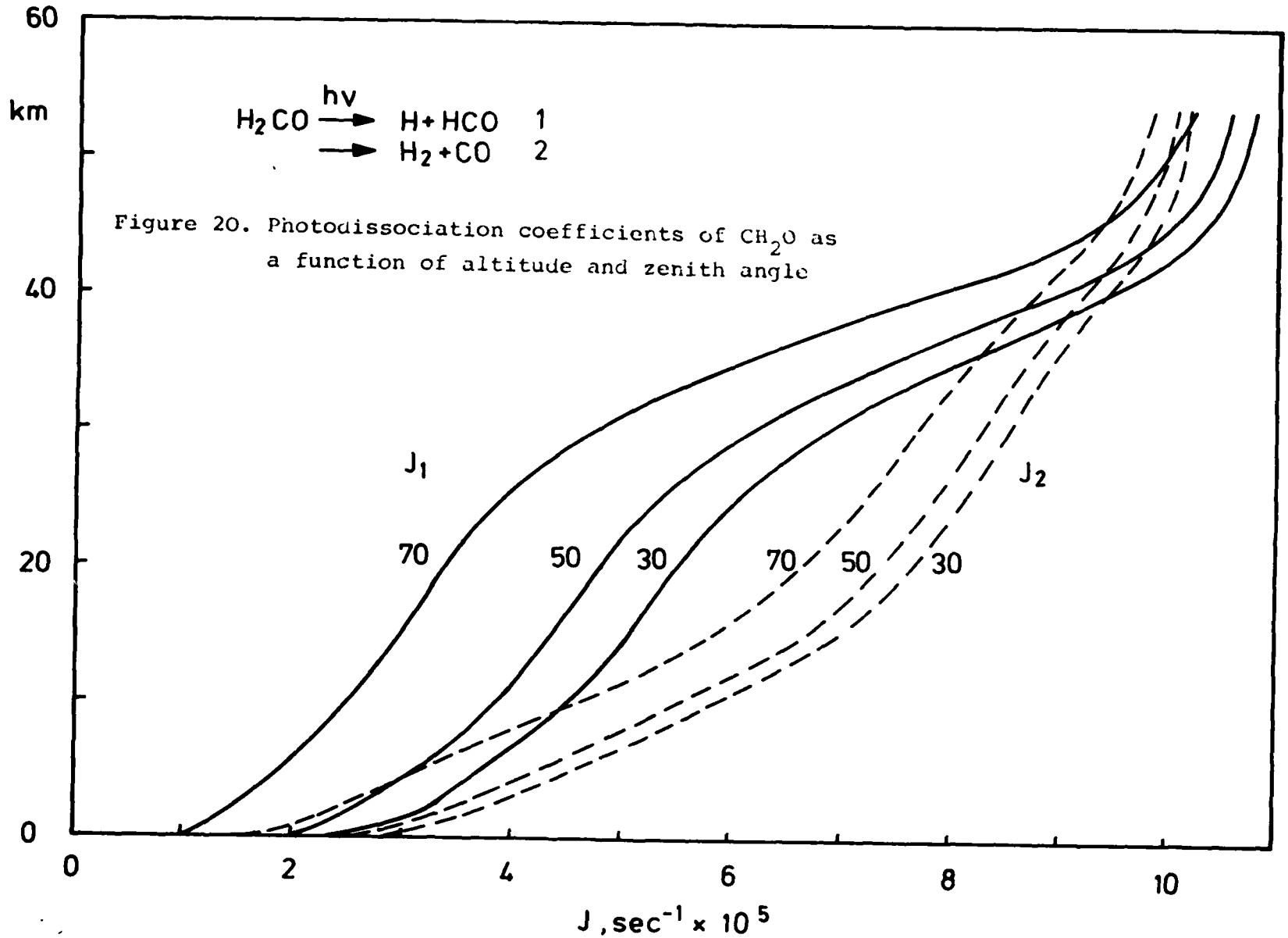

Figure 20. Photodissociation coefficients of CH_2O as a function of altitude and zenith angle

END

DATE
FILMED

4-81

DTIC